geosciences

MDPI

Article

Geochemical, Geological and Groundwater Quality Characterization of a Complex Geological Framework: The Case Study of the Coreca Area (Calabria, South Italy)

Giovanni Vespasiano [1,2,*], Francesco Muto [1] and Carmine Apollaro [1]

[1] Department of Biology, Ecology and Earth Sciences (DiBEST), University of Calabria, P. Bucci, cubo 15b, Arcavacata, 87036 Rende, Italy; mutofr@unical.it (F.M.); apollaro@unical.it (C.A.)
[2] E3 (Environment, Earth, Engineering) Soc. Coop., University of Calabria, P. Bucci, 15b, Arcavacata, 87036 Rende, Italy
* Correspondence: giovanni.vespasiano@unical.it

check for updates

Citation: Vespasiano, G.; Muto, F.; Apollaro, C. Geochemical, Geological and Groundwater Quality Characterization of a Complex Geological Framework: The Case Study of the Coreca Area (Calabria, South Italy). *Geosciences* **2021**, *11*, 121. https://doi.org/10.3390/geosciences11030121

Academic Editors: Nicolo Colombani and Jesus Martinez−Frias

Received: 18 January 2021
Accepted: 3 March 2021
Published: 8 March 2021

Abstract: Hydrogeochemical characterization and statistical methods were used to investigate the groundwater quality and the origin of constituents (anthropic or natural) in groundwater of the Coreca area (Calabria, South Italy). Coreca is characterized by an articulated geological setting where the three main geological complexes that distinguish the Northern Calabria Peloritan Orogen (CPO) outcrop. This complex asset affects the quality of groundwater mainly exploited for irrigation use. In particular, the presence of ultramafic rocks (e.g., serpentinite and metabasite) promotes the release of harmful elements such as Cr and Ni. In the studied area, two groups of waters were identified: Ca-HCO_3 waters strongly controlled by the interaction with Ca-rich phases (e.g., limestone), and Mg-HCO_3 waters related to the interaction of meteoric water with the metamorphic units. Statistical elaboration allowed to detect, in the Mg-HCO_3 group, a good correlation between Cr and Ni (not observed in Ca waters) and a negative correlation between Cr, Ca and Al, in agreement with direct interaction with ultramafic rocks characterized by low concentrations of CaO and Al_2O_3. The concentration of major and trace elements has been compared with the Italian law limit values and the drinking water guidelines provided by the World Health Organization (WHO). Only three samples showed Mn and Ni concentration higher than the Italian law threshold. Furthermore, the assessment of groundwater quality was carried out using salinity and metal indexes. The groundwater quality assessment for irrigation allowed to classify the resource as "excellent to good" and "good to permissible"; nevertheless, a salinity problem and a magnesium hazard were found. Lastly, a metal index (MI) calculation revealed values <1 for almost all samples, pointing to good overall quality. Only a few samples showed a value extremely higher than 1, attributable to prolonged interaction with ultramafic rocks and/or localized anthropogenic pollution. From a general point of view, groundwater showed a generally good quality except for limited areas (and limited to the set of constituents analyzed) and a mild exceedance of the maximum salinity thresholds that must be monitored over time. Through a multidisciplinary approach, it was possible to ascertain the main anomalies attributable to the interaction with the hosting rocks and not (with few exceptions) to anthropic processes.

Keywords: hydrogeochemistry; statistical analysis; Coreca basin; drinking and irrigation use; metal index

1. Introduction

Groundwater composition is closely linked to the geological and structural setting of the hosting aquifer due to physical and chemical characteristics that depend on several factors, such as water–rock interaction processes, residence time, hydrodynamic conditions, and mixing processes [1,2]. Groundwater represents an essential part of water resources for human survival and economic development. In the last century, human activities and environmental changes have imposed significant impacts on groundwater environment [3–8]. In fact, anthropogenic activities associated with rapid urbanization, industrialization, and intensive agricultural activities have caused a deterioration in water quality worldwide. The contamination in groundwater can persist for a long time due to the low flow rate of groundwater in an aquifer and may involve major ions and trace constituents. High levels of contaminants can make water unsuitable for drinking, irrigation, fishing, and recreation [9], causing serious adverse effects on human and biota health [10]. Based on the above, the correct management and characterization of groundwater resources is one of the most challenging current and future issues of global interest.

In areas highlighting a complex geological–structural arrangement, it is not easy to discern geochemical characteristics linked to a mere water–rock interaction from processes induced by human activity [11–14]. In these contexts, multidisciplinary approaches based on geological and geochemical characterization combined with statistical techniques could represent useful tools to reconstruct groundwater evolution and related geochemical processes [11,15].

The aim of this work is the groundwater characterization of the complex geological framework of the Coreca area (Calabria, South Italy) through a multidisciplinary approach. The Coreca area is located near the Tyrrhenian coast, in proximity of the Oliva Catchment (60 km^2 and 19 km in length from NE to SW), which has been site of numerous environmental surveys with the aim to characterize the environmental matrices. Previous surveys, carried out by the competent authorities, highlighted, on the main matrixes, the occurrence of several heavy metals and pollutants such as copper, mercury, zinc, manganese, and other radionuclides for medical and industrial use, higher than Italian law and World Health Organization threshold limits. The complexity of the geological setting and data from historical surveys makes the Coreca area a site of high interest.

Rock and water compositions were elaborated following statistical methods, combined with hydrogeochemical modeling and conventional plots to investigate groundwater and related geochemical processes.

Moreover, according to the critical issues attributable to the proximity to the coast line and the main anthropic activities (mainly agricultural activities and small farms), water composition had been compared with the Italian law limit values of D.Lgs 152/2006 [16], which establishes the lowest threshold of concentration for groundwater, and the drinking-water guidelines provided by the World Health Organization (WHO) [17]. Furthermore, the groundwater salinity, sodium, and magnesium hazards of irrigation water were calculated using the sodium adsorption ratio (SAR) [18], Kelly ratio (KR) [19], magnesium Adsorption ratio (MAR) [20], soluble sodium percentage (SSP) [21], and potential salinity (PS) [22] equations following the general approach proposed by [23]. These indexes have been largely used for determining the suitability of groundwater for a proper agricultural use [10,23–26]. Finally, the metal index (MI) was calculated to assess the water quality with respect to heavy metals.

A final hydrogeochemical conceptual model was reconstructed and reported on summary schematic sections.

2. Geological Framework

The Calabrian Peloritan Orogen (CPO) represents a fragment of the European margin, which was thrust onto the Maghrebian-Sicilian and Apennine thrust-and-fold belts during the Europe-Apulia collision in the Oligocene–Early Miocene [27–30]. With crystalline and metamorphic rocks, overthrusted on sedimentary deposits of the southern Apennine, the CPO is one of the most fascinating areas of south Italy.

The CPO has been divided in two sectors (Northern and Southern) separated by a strike-slip tectonic line running along the Catanzaro Trough [31–38].

The Northern sector has been divided into the following three main tectonic complexes [39], from bottom to top: (i) the Apennine Units Complex, consisting of Mesozoic sedimentary and metasedimentary successions (Trias–Miocene) [40–42]; (ii) the allochthonous

Alpine Liguride Complex (Tithonian–Neocomian), consisting of a series of Alpine metamorphic units including a Cretaceous–Paleogene metapelitic-ophiolitic-carbonate assemblage [27]; (iii) the Calabride Complex, made up of Hercynian and pre-Hercynian gneiss, granite, and metapelite [27–43].

The studied area is localized in the Northern sector of the region, in proximity of the Tyrrhenian coast, and includes the Coreca town (west side), the Gallo town (east side), the Oliva River (southern boundary), and the Coloncì Torrent (northern boundary) (Figure 1). The main anthropogenic activities (sources) consist mainly of farming (olive groves and private crops), olive presses, and chicken farming. The area is close to the Neogene-Quaternary Amantea Basin, located on the western side of the coastal range. The basin developed during the extensional tectonic phase and the consequent opening of the back-arc Tyrrhenian Basin [44–48], simultaneously with compression and accretionary processes, developed in the eastern margin of Calabria [27,49–51].

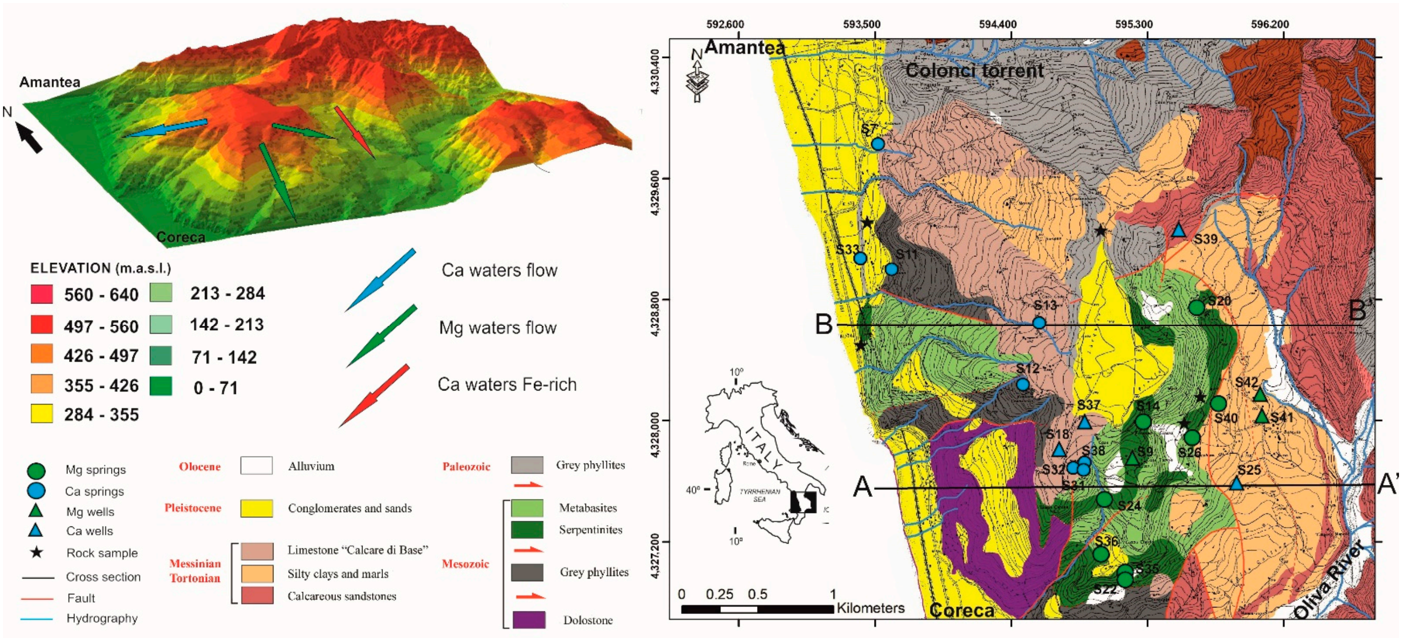

Figure 1. Geological and elevation map of the Coreca area showing locations of wells and springs.

From a geological point of view, the Mesozoic Apennine Unit outcrops in a fault-bounded tectonic window. The Apennine Unit consists of Triassic dolostone and dolomitic limestone (Verbicaro Unit) [42,43] and is overthrusted by the ophiolitic sequence (allochthonous Alpine Liguride) belonging to the Frido (mainly metapelites and slates) and the Gimigliano-Monte Reventino Units (serpentinites, metabasalts, phyllites, and carbonates) [52,53]. The metamorphic units are sealed by the Miocene sedimentary sequences consisting of calcareous sandstones, calcarenites, clays, marls, and Messinian limestone ("Calcare di base"). Pleistocene terraced deposits, consisting of conglomerates and sands, outcrop at the top of the succession.

The hydrogeology of the Coreca area is characterized by two different kinds of aquifers: fissured aquifers in the metamorphic units and partially in the Miocene deposits, and porous multilayer aquifers developed in the Miocene/Quaternary successions. Both types present relatively high volumes of groundwater storage and circulation, with the richest amount located in the fractured–altered superficial portion of the metamorphic units characterized by high permeability. Porous aquifers occur in gravelly–sandy permeable deposits of the quaternary succession, with flowrates variable according to annual rainfall. As reported by [54–60], Mesozoic limestone (Apennine Unit) represents the main thermal aquifer of the region and one of the main sources of drinking water supplies in Calabria and Southern Italy. However, in the Coreca area, Mesozoic successions do not highlight thermal evidence, with much less developed surface aquifers due to the high fracturing.

3. Methods

A total of 23 groundwater samples, from 2011 to 2014, were collected and analyzed for major cations, anions, and trace elements. Furthermore, 9 representative rock samples were collected and analyzed.

Water samples were collected from 16 springs and 7 wells (the location for each sample is reported in Figure 1).

Chemical–physical parameters such as pH, Eh, temperature, alkalinity, and specific electrical conductivity were measured in the field by means of portable instruments (HI-9828). Two pH buffers, with nominal pH values of 4.01 and 7.01 at 25 °C, were used for pH calibration. The ZoBell's solution [61] was used to calibrate the mV-meter for Eh measurement. Total alkalinity was determined by acidimetric titration, using HCl 0.05N as titrating agent and methylorange as indicator.

In the laboratory, the concentrations of F, Cl, Br, SO_4, NO_3, PO_4, Na, K, Mg, and Ca were determined by HPLC (DIONEX DX 120). During the same day, it was measured dissolved reactive SiO_2 by VIS spectrophotometry upon reaction with ammonium molybdate in acid media (and treatment with oxalic acid) to form a yellow silicomolybdate complex, whose absorbance was read at 410 nm [62]. Trace elements were analyzed by a quadrupole ICP-MS (Perkin Elmer/SCIEX, Elan DRCe) with a collision reaction cell capable of reducing or avoiding the formation of polyatomic spectral interferences. Data quality for major components was estimated by charge balance. Deviation between the sum of cation concentrations and the sum of anion concentrations, both in equivalent units, varied between −5% and +5%. Data quality for minor and trace elements was checked by running the NIST1643e standard reference solution. Deviations from the certified concentrations were found to be lower than 5%. The results of laboratory analyses and field data are shown in Tables 1 and 2. For each sample, the saturation index (SI), with respect to the mineral phases, was performed using PHREEQC Interactive software, version 3.1.1 [63] using the LLNL thermodynamic database.

The mineralogical associations for each main lithotype were determined using an optical microscope and by means of a Bruker D8 Advance XRD Diffractometer.

Table 1. Location, physical–chemical parameters, and concentrations of major elements of water samples. The limit values according to the D.Lgs. 152/2006 and the World Health Organization [WHO] drinking-water guidelines are shown. d.l. = detection limit.

Sample	**X**	**Y**	**Date**	**Type**	**pH**	**Eh**	**EC**	**T**	**Ca**	**Mg**	**K**	**Na**	**Cl**	**SO_4**	**HCO_3**	**F^-**	**NO_3**	**SiO_2**
						mV	**µS/cm**	**°C**	**mg L^{-1}**	**mg L^{-1}**	**mg L^{-1}**	**mg L^{-1}**	**mg L^{-1}**	**mg L^{-1}**	**mg L^{-1}**	**mg L^{-1}**	**mg L^{-1}**	**mg L^{-1}**
D.Lgs. 152/2006					-	-	-	-	-	-	-	-	**250**	**250**	-	**1.5**	**50**	
(WHO)					-	-	-	-	-	-	-	-	**250**	**500**	-	**1.5**	**50**	
S7	593535	4329798	30/06/2011	Spring	7.02	0.89	971	18.8	108.12	10.88	3.01	38.73	39.67	103.43	393.86	0.64	12.64	21.75
S11	593627	4328990	30/06/2011	Spring	7.97	0.57	846	20.2	105.40	18.42	2.61	40.32	53.05	58.23	320.29	0.53	19.39	20.50
S12	594551	4328176	30/06/2011	Spring	7.53	0.83	796	17.8	91.80	21.50	1.87	22.01	25.10	30.35	368.85	0.69	42.51	23.75
S13	594605	4328669	30/06/2011	Spring	7.25	0.71	660	18.6	65.29	29.94	0.64	29.29	34.62	21.09	339.25	0.42	<d.l.	21.25
S14	595264	4327973	30/06/2011	Spring	7.47	0.97	617	18.4	50.84	33.83	1.97	32.11	36.29	22.35	294.41	0.30	3.00	26.75
S20	595654	4328741	02/07/2011	Spring	7.44	131	728	16.4	54.29	41.79	0.50	21.43	36.10	49.93	348.71	0.30	<d.l.	38.00
S22	595132	4326907	02/07/2011	Spring	8.06	136	1178	20.06	54.66	55.38	2.18	98.43	103.99	66.73	471.36	1.19	<d.l.	16.50
S24	595013	4327465	02/07/2011	Spring	7.13	114	938	18.5	56.55	43.58	2.22	39.73	44.84	41.31	401.19	<d.l.	<d.l.	32.00
S2	595587	4327873	02/07/2011	Spring	7.22	178	767	17.5	64.67	39.97	1.47	38.53	44.63	28.69	393.56	0.36	<d.l.	30.25
S31	594923	4327588	03/07/2011	Spring	7.48	0.95	846	18.5	74.34	30.99	3.01	36.66	39.63	39.96	393.56	<d.l.	<d.l.	20.00
S32	594938	4327623	03/07/2011	Spring	7.92	174	891	20.3	99.93	43.66	0.55	41.30	37.38	36.79	471.36	0.56	<d.l.	14.50
S33	593418	4329062	03/07/2011	Spring	7.94	0.97	997	20.4	112.10	20.95	5.99	54.74	76.78	63.86	378.31	0.59	24.49	21.25
S35	595136	4326966	03/07/2011	Spring	7.9	129	1007	22.3	47.65	46.92	1.00	84.45	80.68	44.83	457.70	<d.l.	<d.l.	15.75
S36	594975	4327089	03/07/2011	Spring	7.32	132	855	20.3	48.51	48.72	1.38	40.30	46.21	54.82	355.42	<d.l.	<d.l.	40.00
S38	594862	4327587	03/07/2011	Spring	6.91	77	986	18.9	137.91	21.30	4.30	39.90	55.26	48.85	402.71	0.45	32.35	14.00
S40	595758	4328100	04/07/2011	Spring	6.98	0.56	1056	24.6	90.84	64.21	1.52	52.66	58.18	40.00	538.29	0.57	10.12	20.32
S9	595221	4327737	16/07/2014	Well	7.33	0.17	853	24.2	38.09	52.20	2.72	32.61	43.96	49.01	360.95	<d.l.	<d.l.	29.06
S18	594755	4327722	16/07/2014	Well	6.86	176	1124	19	135.38	24.99	6.99	36.27	46.53	115.31	361.53	0.39	13.58	24.25
S25	595930	4327581	16/07/2014	Well	7.23	−100	1263	22.5	89.84	40.51	4.42	73.36	68.24	212.06	334.07	0.38	<d.l.	16.25
S37	594906	4327946	01/09/2014	Well	7.21	174	796	17.6	62.99	28.26	0.50	44.73	24.51	39.53	399.66	<d.l.	<d.l.	21.00
S39	595512	4329250	01/09/2014	Well	7.3	−152	1071	21.5	124.67	34.58	15.90	40.65	40.14	183.79	357.82	0.54	<d.l.	11.06
S41	596071	4327972	16/07/2014	Well	7.02	30	700	19.5	48.35	46.94	2.69	28.03	35.59	45.01	334.28	0.51	0.56	36.01
S42	596044	4328108	16/07/2014	Well	7.06	14	943	19	64.32	43.04	0.55	59.44	67.65	82.16	357.82	0.27	1.98	31.89

Table 2. Concentrations of trace elements of the water samples analyzed. The limit values according to the D.Lgs. 152/2006 and the World Health Organization (WHO) drinking-water guidelines are shown. Values that exceeded drinking-water guidelines are shown in bold. d.l. = detection limit; *MI* = metal index.

Sample	Li	B	Al	V	Cr	Mn	Co	Ni	Cu	Zn	Sr	Se	Mo	U	Pb	As	Cd	Ba	Sb	Fe	MI
	$\mu g\ L^{-1}$	$\mu g\ L^{-1}$	$\mu g\ L^{-1}$	$\mu g\ L^{-1}$	$\mu g\ L^{-1}$	$\mu g\ L^{-1}$	$\mu g\ L^{-1}$	$\mu g\ L^{-1}$	$\mu g\ L^{-1}$	$\mu g\ L^{-1}$	$\mu g\ L^{-1}$	$\mu g\ L^{-1}$	$\mu g\ L^{-1}$	$\mu g\ L^{-1}$	$\mu g\ L^{-1}$	$\mu g\ L^{-1}$	$\mu g\ L^{-1}$	$\mu g\ L^{-1}$	$\mu g\ L^{-1}$	$\mu g\ L^{-1}$	
D.Lgs. 152/2006	-	***1000***	***200***	-	***50***	***50***	***50***	***20***	***1000***	***3000***	-	***10***	-	-	***10***	***10***	***5***	-	***5***	-	
(WHO)	-	-	***200***	-	***50***	***400***	-	***70***	***2000***	***4000***	-	***40***	-	-	***10***	***10***	***3***	-	***20***	-	
S7	7.92	39.73	3.6	0.38	<d.l.	<d.l.	<d.l.	0.51	0.62	6.52	51950.63	<d.l.	11.18	5.44	0.05	0.47	0.04	98.38	<d.l.	11.32	0.38
S11	4.93	42.01	1.53	1.08	1.95	<d.l.	<d.l.	1.09	0.44	1.41	22765.72	<d.l.	0.86	2.76	0.08	0.8	0.01	237.52	<d.l.	13.99	0.53
S12	1.95	19.97	3.64	0.61	1.58	<d.l.	<d.l.	3.08	0.63	7.82	345.12	0.9	0.63	1.91	0.06	1.05	0.01	259.04	<d.l.	10.64	0.58
S13	5.8	20.46	<d.l.	0.81	<d.l.	<d.l.	<d.l.	0.97	0.21	56.71	206.45	1.22	1.99	1.89	0.03	0.45	<d.l.	45.49	<d.l.	6.28	0.32
S14	5.65	25.53	3.84	10.06	3.53	<d.l.	<d.l.	0.07	0.52	4.68	122.06	1.43	<d.l.	0.37	0.14	0.6	<d.l.	4.14	<d.l.	9.18	0.51
S20	3.28	30.56	<d.l.	3.45	7.17	<d.l.	<d.l.	**63.58**	0.45	10.62	125.19	0.92	1.34	1.08	<d.l.	0.71	<d.l.	70.13	0.63	4.63	0.4
S22	21.42	82.9	1.75	0.31	<d.l.	2.13	<d.l.	1.02	0.53	0.17	281.11	2.67	2.66	2.65	0.01	0.76	<d.l.	10.93	0.2	7.24	0.33
S24	7.31	58.73	<d.l.	7.42	6.05	<d.l.	<d.l.	3.89	0.52	1.79	345.99	1.34	<d.l.	2.55	<d.l.	0.95	<d.l.	36.21	<d.l.	8.32	0.34
S26	3.24	33.63	6.31	1.57	5.68	3.35	<d.l.	2.5	0.49	2.64	199.14	0.92	0.93	1.49	0.04	0.73	<d.l.	7.58	<d.l.	9.84	**1.03**
S31	6.97	43.78	4.47	7.34	<d.l.	<d.l.	<d.l.	0.57	0.54	2.43	577.32	1.36	1.5	3.75	0.09	1.25	<d.l.	164.91	<d.l.	5.87	**117.6**
S32	6.79	46.58	3.82	4.52	<d.l.	1.38	<d.l.	0.43	0.37	8.64	555.79	0.56	1.75	3.5	<d.l.	0.82	<d.l.	148.23	<d.l.	4.82	0.45
S33	5.98	47.5	2.97	1.44	<d.l.	<d.l.	<d.l.	0.74	0.63	24.54	21086	<d.l.	1.33	3.15	0.02	0.99	<d.l.	193.78	<d.l.	4.17	**155.02**
S35	18.15	74.22	5.75	0.38	<d.l.	8.46	<d.l.	0.39	0.46	3.7	248.46	1.03	1.37	1.33	0.06	0.51	<d.l.	9.65	<d.l.	32.15	0.61
S36	12.99	60.6	<d.l.	11.84	5.37	<d.l.	<d.l.	7.34	0.48	14.2	343.24	2.29	0.92	1.77	0.15	1.55	<d.l.	29.17	<d.l.	5.85	**3.73**
S38	5.1	51.79	4.33	0.35	<d.l.	<d.l.	<d.l.	0.12	0.52	6.01	974.76	1.89	0.65	5.09	0.08	0.5	<d.l.	206.02	0.15	8.67	0.4
S40	10.95	38.23	3.32	12.59	<d.l.	<d.l.	<d.l.	0.13	3.51	13.02	108.96	4.68	<d.l.	0.32	<d.l.	0.37	<d.l.	2	<d.l.	9.12	0.8
S9	16.77	60.05	6.06	16.13	4.93	1.18	<d.l.	6.04	2.31	9.01	425.94	1.82	<d.l.	1.45	0.45	1.17	<d.l.	24.85	<d.l.	10.49	0.69
S18	17.05	119.48	3.28	0.22	<d.l.	<d.l.	<d.l.	1.65	2.7	5.31	5845.6	1.53	10.42	4.75	0.2	1.5	0.02	41.74	2.73	9.06	0.98
S25	15.24	196.89	82.72	0.04	<d.l.	**111.64**	0.46	1.38	1.84	0.23	3311.05	0.98	0.1	0.2	1.07	0.62	<d.l.	19.7	<d.l.	**5733**	**1.06**
S37	5.79	31.71	7.98	0.94	1.5	1.35	<d.l.	1.09	1.13	5.66	303.77	3.49	1.93	3.45	0.18	0.69	<d.l.	52.9	0.14	6.68	0.57
S39	38.05	46.25	6.27	0.31	<d.l.	**66.02**	0.49	1.4	0.98	10.1	569.17	<d.l.	<d.l.	9.96	0.02	0.72	<d.l.	76.14	<d.l.	**7673**	**1.2**
S41	2.13	50.8	4.64	2.98	1.73	3.73	<d.l.	1.17	1.43	5.43	242.99	2.06	<d.l.	1.78	0.06	1.02	<d.l.	10.59	<d.l.	11.35	0.64
S42	1.52	45.08	5.32	2.58	<d.l.	7.27	<d.l.	1.8	1.4	90.99	350.71	2.68	7.23	1.34	0.33	0.62	0.11	20.56	<d.l.	9.18	0.68

4. Results and Discussion

4.1. Mineralogical Characteristics

To characterize the main outcropping lithotypes, samples of metabasalts, serpentinites, and phyllites were collected for mineralogical analyses.

Optical microscopy observations and XRD analyses indicated that: (i) metabasalts, outcropping in the Coreca area, consisted mainly of chlorite, epidote, actinolite, and albite, with small amounts of calcite; (ii) serpentinites were composed of fine-grained crystals of serpentine minerals (antigorite as primary phase, as also reported by [64]), with subordinate magnetite; (iii) phyllites were made up of white mica and albite with significant amounts of chlorite and quartz, and small amounts of calcite.

4.2. Physical–Chemical Parameters

Springs (n = 16) and wells (n = 7) collected in the Coreca area (Figure 1) showed an average temperature of 19.5 ± 2 °C and 20.5 ± 2.4 °C, respectively, which were slightly higher than the yearly mean atmospheric temperature (15.6 ± 5.3 °C). The pH and EC (electrical conductivity) values were comparable between springs and wells and showed average values of 7.47 ± 0.38 and 983 ± 149 (µS/cm) and 7.14 ± 0.17 and 964 ± 198 (µS/cm), respectively. Overall, Eh showed a wide positive range of values both for springs and wells, with only samples S25 and S39 highlighting negative values (Table 1).

4.3. Geochemical Characteristics

Water chemistry was investigated by using: (i) triangular plots involving major cations and major anions (Figure 2), both prepared starting from the concentrations in equivalent units; (ii) a correlation graph for SO_4 vs. HCO_3 + Cl, in which iso-salinity lines were drawn for reference (Figure 3); (iii) box and whisker plots (Figure 4);

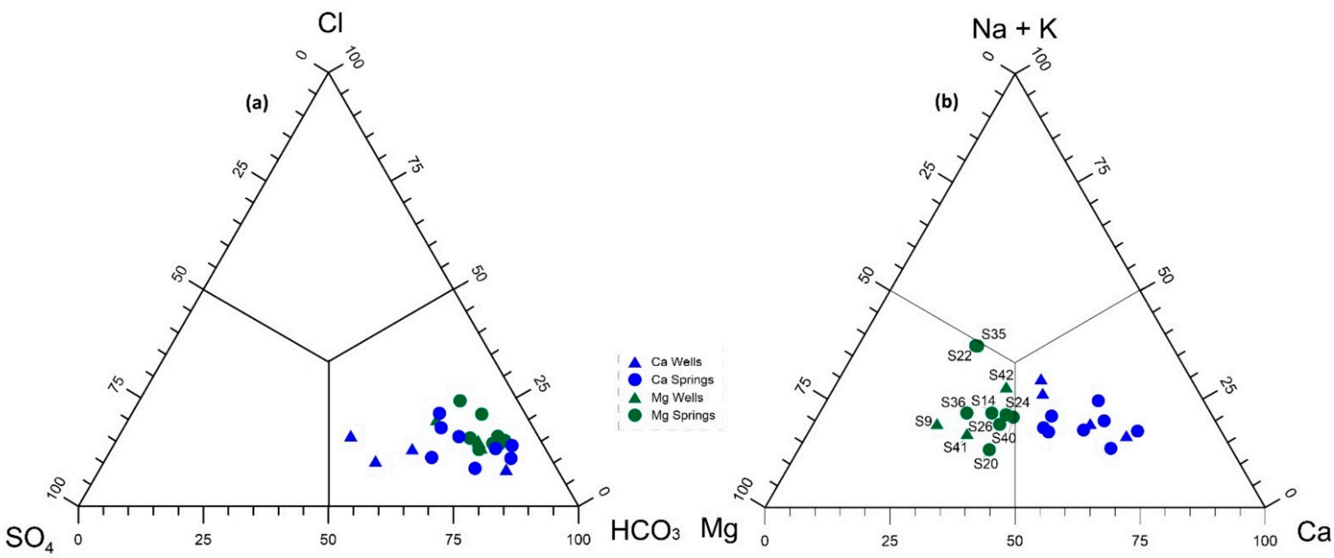

Figure 2. Triangular diagrams of (**a**) major anions and (**b**) major cations for the Coreca waters.

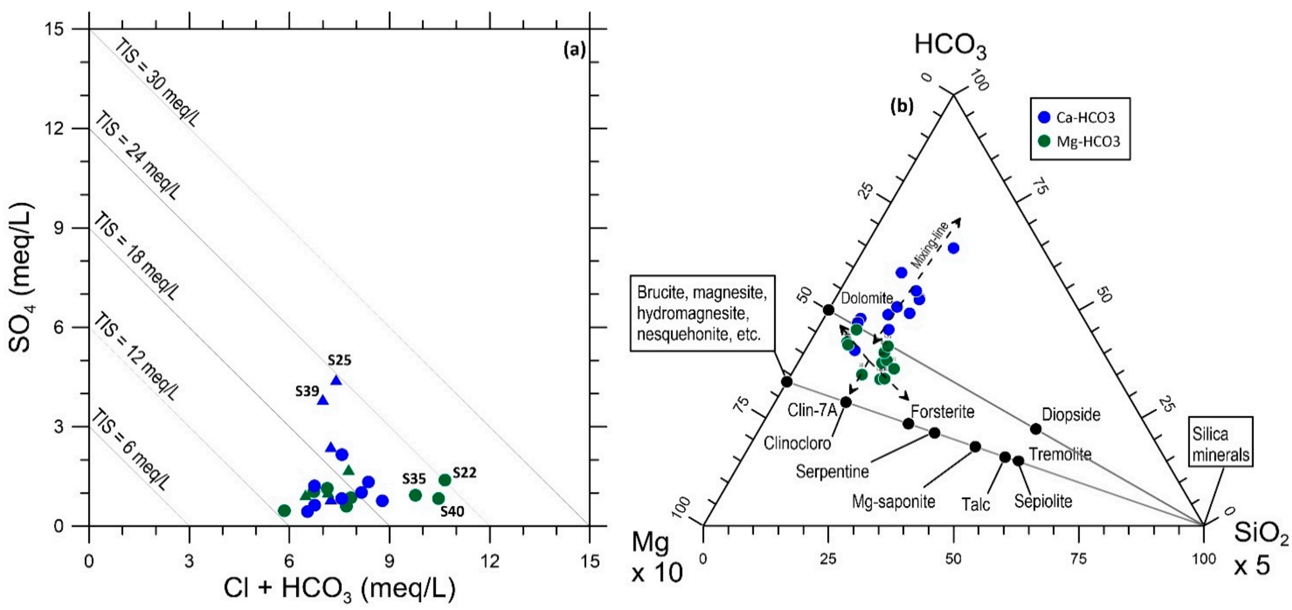

Figure 3. (**a**) SO_4 vs. HCO_3 + Cl (TIS) plot and (**b**) triangular diagrams (HCO_3 + CO_3)-Mg-SiO_2 reporting the samples collected in the Coreca area. In the TIS diagram, the iso-ionic-salinity lines are drawn as reference.

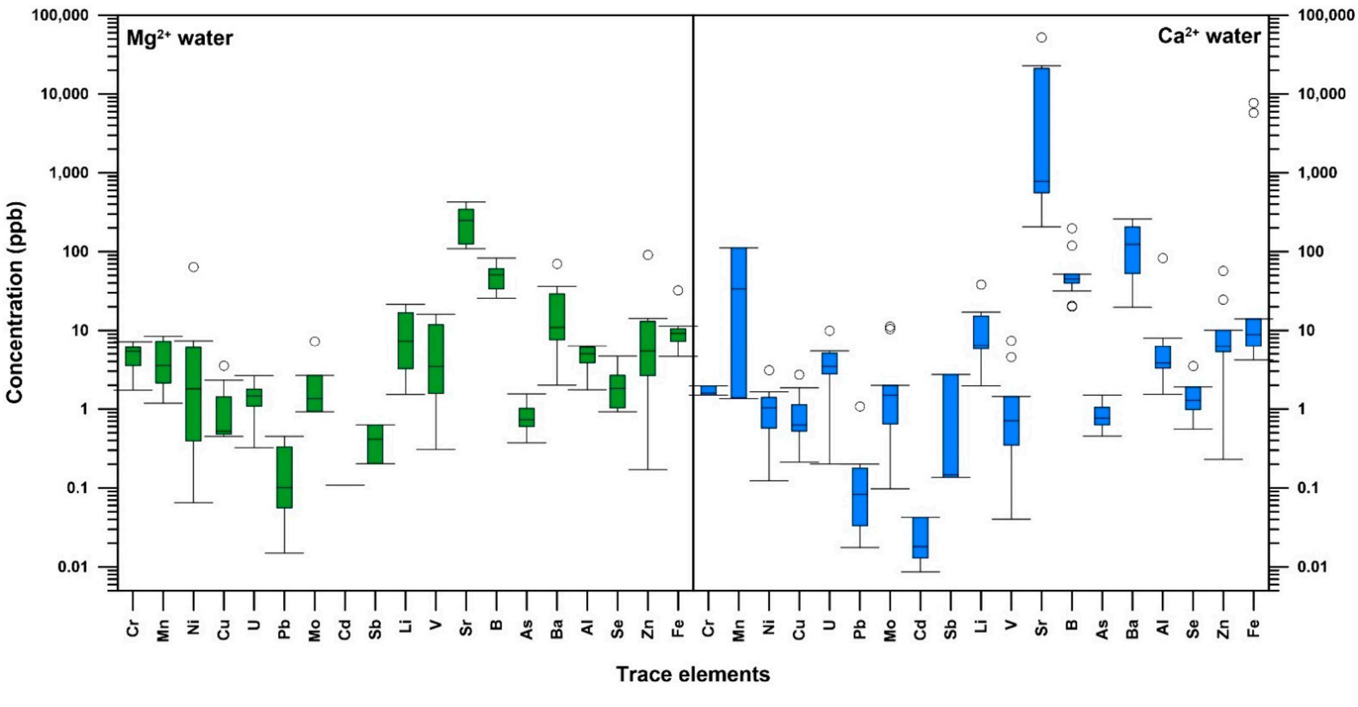

Figure 4. Box and whisker plot for the distribution of trace elements in waters.

Triangular plots (Figure 2) allowed to identify two groups of waters. The first group had a Ca-HCO_3 composition suggesting a chemism controlled by dissolution of Ca-rich phases and/or other processes such as ionic exchange. Among the Ca-bearing phases, calcite, which occurs both in metabasalts and carbonatic rocks, represents the phase with the highest dissolution rates. Its presence promotes Ca-HCO_3 waters [12,65,66]. The second group had a Mg(Ca)-HCO_3 composition, probably due to the interaction with ultramafic rocks and/or carbonate-dolomitic successions, where antigorite, actinolite (in serpentinite and metabasalt), and dolomite are the local phases that can promote formation of Mg-HCO_3 waters [5,12,67].

Triangular diagrams represent a useful tool to define the main geochemical groups. Unfortunately, no information about salinity was provided. To cope with this, samples were also classified using the TIS diagram (SO_4 vs. HCO_3 + Cl, Figure 3a), in which comparable salinity values between 12 meq/L to 24 meq/L are evident for the two groups of water. Salinity values and ratios of major constituents obtained in S22, S40, and S35 samples, belonging to Mg-HCO_3 waters, suggested a prolonged water–rock interaction with the hosting units (see below and Table 3), increasing their salinity and Mg concentration. Furthermore, the S25 and S39 samples (Ca—deep wells) highlighted a considerable sulphate increase and high Fe (5733 and 7673, respectively) and Mn (112 and 76, respectively) concentration. These samples were representative of a third aquifer (Ca waters, Fe-rich), hosted in the calcareous sandstone directly in contact (tectonic contact) with the metamorphic basement (grey phyllites). This aquifer is isolated from the Ca-rich and Mg-rich systems due to the presence of the normal fault system (N-S), which put in contact (aquiclude) the Tortonian-Messinian filling to the east (the aquifer) with the metamorphic basement to the west. The anomalies were probably due to repeated alternations of reducing and oxidizing conditions that can promote dissolution of sulfides and Fe-Mn oxy-hydroxides.

With the aim to improve the knowledge about processes and evolution undergone by the considered systems, for each sample, the saturation index (SI), with respect to specific mineral phases, was performed using PHREEQC Interactive software, version 3.1.1 [63] using the LLNL thermodynamic database. Geochemical data were elaborated by using of the triangular plot for (HCO_3 + CO_3)-Mg-SiO_2 reported in Figure 3b [68]. Unlike previous triangular diagrams, the triangular plot (HCO_3 + CO_3)-Mg-SiO_2 in Figure 3b was prepared starting from the concentrations in weight units. The diagram allowed to compare the observed compositions with those expected for congruent dissolution of different magnesian minerals, such as serpentine, talc, sepiolite, brucite, and magnesite (and other carbonates); and for incongruent dissolution of Mg saponite and clinochlore (accompanied by precipitation of Al-secondary silicates). The compositions expected for dissolution of these solid phases were represented based on the stoichiometric coefficients of the relevant reactions.

This triangular plot is useful in areas with lithotypes characterized by Mg-bearing phases such as metabasites (chlorites) and serpentinites. With the diagram, an attempt was made to discriminate whether the Mg system belonged to the metabasite or serpentinite aquifer, or at least where the predominant circulation and interaction occurred.

Water–rock interactions with the specific phases are shown in Figure 3b. Mg-HCO_3 waters fell between the compositions expected for dissolution of clinochlore and calcite, suggesting a prevailing interaction with rocks holding these two phases (e.g., metabasite). A shift toward phases linked to ultramaphic rocks was only mildly evident. Hydrogeological evidence confirmed the geochemical data that allowed the exclusion of Mg compositions linked to an interaction with the dolomitic successions (see Section 5). Ca-HCO_3 fell above the dolomite–diopside line, suggesting an interaction with carbonate phases.

As reported in Table 3, most waters reached oversaturation with calcite, dolomite, clinochlore, tremolite, and albite, and reached values close to the saturation with phases characterizing the main outcropping lithotypes. Samples S22 and S35 showed the highest SI values with respect to clinochlore, albite, and tremolite, directly linked to metabasites, and phases characterizing ultramafic rocks (e.g., antigorite).

4.4. Statistical Analysis

Elements concentration and distribution were elaborated by a statistical approach based on box and whisker plots (Figure 4) and Pearson's correlation coefficients (Tables 4 and 5).

Table 3. Saturation indices (SI) for main mineral phases in both water types. Mg waters are in bold. The last two lines show the averages of the saturation indices for each geochemical group. In Bold Mg-HCO_3 waters.

ID	pH	Clinochlore 14A	Clinochlore 7A	Albite	Albite High	Albite Low	Tremolite	Calcite	Dolomite	Dolomite Dis	Dolomite Ord	Magnesite	Antigorite	Forsterite	Saponite Mg	Talc	Sepiolite
S7	7.02	−8.54	−11.97	0.46	−0.90	0.46	−15.23	0.12	0.61	−0.98	0.61	−1.18	−103.46	−11.11	−3.31	−3.94	−9.63
S11	7.97	0.01	−3.40	0.07	−1.28	0.07	−0.61	0.99	2.60	1.02	2.61	−0.05	1.39	−6.67	3.11	2.50	−1.10
S12	7.53	−2.58	−6.01	0.56	−0.81	0.56	−6.50	0.53	1.81	0.22	1.82	−0.40	−39.56	−8.51	0.88	0.17	−4.11
S13	7.25						−10.05	0.11	1.25	−0.33	1.26	−0.52	−58.70	−9.25		−1.15	−5.92
S31	7.48	−2.13	−5.56	0.58	−0.78	0.58	−7.02	0.44	1.86	0.28	1.87	−0.24	−37.93	−8.38	0.89	0.10	−4.27
S32	7.92	1.80	−1.61	0.02	−1.33	0.01	−0.72	1.07	3.16	1.59	3.17	0.44	9.31	−6.28	3.56	2.71	−0.92
S33	7.94	0.63	−2.78	0.52	−0.83	0.52	−0.61	1.04	2.74	1.16	2.75	0.04	1.51	−6.67	3.24	2.53	−1.05
S38	6.91	−8.40	−11.82	−0.08	−1.44	−0.08	−16.55	0.12	0.81	−0.77	0.82	−0.98	−105.81	−11.13	−3.70	−4.45	−10.44
S18	6.86	−8.09	−11.51	0.45	−0.91	0.44	−15.07	0.01	0.66	−0.93	0.67	−1.02	−99.72	−10.97	−2.99	−3.62	−9.18
S25	7.23	−1.08	−4.48	1.52	0.19	1.52	−9.96	0.20	1.42	−0.13	1.43	−0.42	−54.59	−8.88	−0.02	−1.27	−6.24
S37	7.21	−4.13	−7.57	1.02	−0.35	1.01	−11.15	0.10	1.21	−0.38	1.22	−0.56	−66.66	−9.62	−0.77	−1.62	−6.52
S39	7.3	−3.70	−7.10	−0.27	−1.61	−0.27	−10.56	0.43	1.67	0.10	1.68	−0.41	−58.41	−9.01	−0.86	−1.78	−7.02
S40	6.98	−4.20	−7.58	0.05	−1.27	0.05	−10.98	0.21	1.67	0.13	1.68	−0.17	−59.83	−9.05	−0.71	−1.49	−6.54
S14	7.47	−1.67	−5.10	0.85	−0.51	0.85	−6.14	0.16	1.52	−0.07	1.53	−0.31	−31.81	−8.18	1.46	0.72	−3.35
S20	7.44						−5.44	0.19	1.61	0.01	1.62	−0.25	−30.13	−8.26		1.19	−2.57
S22	8.06	2.80	−0.61	0.24	−1.12	0.23	1.49	0.92	3.24	1.66	3.24	0.66	28.22	−5.52	4.74	4.00	0.84
S24	7.13						−9.78	−0.02	1.21	−0.38	1.22	−0.43	−57.53	−9.28		−0.74	−5.25
S26	7.22	−3.05	−6.49	1.33	−0.04	1.33	−8.99	0.11	1.37	−0.23	1.37	−0.41	−53.28	−9.13	0.30	−0.48	−4.89
S35	7.9	2.56	−0.84	0.46	−0.88	0.46	−0.72	0.75	2.89	1.33	2.90	0.50	14.10	−6.01	3.91	3.00	−0.56
S36	7.32						−5.82	0.08	1.53	−0.04	1.54	−0.20	−30.12	−8.11		1.08	−2.80
S41	7.02	−4.14	−7.56	1.06	−0.29	1.06	−10.59	−0.25	0.85	−0.72	0.86	−0.55	−62.39	−9.46	−0.28	−0.99	−5.57
S42	7.06	−4.20	−7.62	1.35	−0.01	1.35	−10.67	−0.09	1.01	−0.58	1.01	−0.56	−64.32	−9.54	−0.44	−1.19	−5.86
S9	7.33	−0.61	−3.99	0.69	−0.63	0.69	−5.91	0.05	1.63	0.09	1.64	−0.05	−24.57	−7.66	1.85	1.02	−3.07
Ca-HCO_3		−3.29	−6.71	0.44	−0.91	0.44	−8.67	0.43	1.65	0.07	1.66	−0.44	−51.05	−8.87	0.00	−0.82	−5.53
Mg-HCO_3		−1.56	−4.97	0.75	−0.59	0.75	−6.69	0.19	1.68	0.11	1.69	−0.16	−33.79	−8.20	1.35	0.56	−3.60

Table 4. Pearson's correlation factor among physical–chemical parameters for major and trace elements of the Ca-water samples. The significant direct and inverse correlations are shown in bold.

	Means	**Std. Dev.**	**Ca**	**Mg**	**K**	**Na**	**Cl**	**SO_4**	**HCO_3**	**SiO_2**	**pH**	**T**	**EC**	**Eh**	**Cr**	**Mn**	**Ni**	**Cu**	**U**	**Pb**	**Mo**	**Li**	**V**	**Sr**	**B**	**As**	**Ba**	**Al**	**Zn**	**Fe**
Ca	100.65	25.11	**1.00**																											
Mg	27.17	9.44	−0.27	**1.00**																										
K	4.15	4.25	**0.60**	0.09	**1.00**																									
Na	41.50	12.77	0.04	0.36	0.16	**1.00**																								
Cl	45.08	15.91	0.43	−0.03	0.27	**0.73**	**1.00**																							
SO_4	79.44	62.34	0.36	0.27	**0.69**	**0.63**	0.41	**1.00**																						
HCO_3	376.77	40.22	0.03	0.23	−0.26	−0.12	−0.27	−0.38	**1.00**																					
SiO_2	19.13	4.16	−0.29	**−0.55**	−0.47	−0.34	−0.18	−0.40	−0.25	**1.00**																				
pH	7.38	0.39	−0.21	0.17	−0.18	0.07	0.19	−0.31	0.10	−0.03	**1.00**																			
T	19.51	1.49	0.31	0.48	**0.52**	**0.73**	**0.66**	**0.76**	−0.25	**−0.60**	0.25	**1.00**																		
EC	937.25	165.56	**0.60**	0.19	**0.58**	**0.69**	**0.63**	**0.87**	−0.13	−0.34	−0.29	**0.70**	**1.00**																	
EH	29.49	104.50	−0.01	−0.02	**−0.53**	−0.24	−0.30	−0.55	**0.58**	0.32	−0.08	−0.55	−0.26	**1.00**																
Cr	0.53	0.70	−0.28	−0.31	−0.34	−0.26	−0.34	−0.34	−0.27	0.36	0.34	−0.33	−0.44	0.13	**1.00**															
Mn	15.15	35.77	0.03	**0.54**	0.48	**0.70**	0.36	**0.88**	−0.37	**−0.52**	−0.14	**0.79**	**0.69**	**−0.63**	−0.24	**1.00**														
Ni	1.09	0.77	−0.09	−0.03	0.11	−0.28	−0.31	0.13	−0.42	0.39	0.01	−0.11	−0.01	−0.19	0.48	0.17	**1.00**													
Cu	0.88	0.72	0.31	0.15	0.34	0.35	0.19	**0.61**	−0.26	0.17	−0.50	0.22	**0.69**	0.16	−0.15	0.40	0.33	**1.00**												
U	3.82	2.43	**0.55**	−0.10	**0.76**	−0.23	−0.16	0.28	0.18	−0.46	−0.27	0.08	0.20	−0.15	−0.28	0.00	−0.19	0.02	**1.00**											
Pb	0.16	0.29	−0.13	0.41	−0.01	**0.76**	0.41	**0.65**	−0.34	−0.13	−0.22	**0.54**	0.63	−0.27	−0.11	**0.80**	0.15	**0.55**	−0.48	**1.00**										
Mo	2.72	3.83	0.29	−0.46	−0.01	−0.19	−0.12	0.10	0.09	0.48	−0.50	−0.28	0.19	0.35	−0.25	−0.30	−0.08	0.42	0.21	−0.13	**1.00**									
Li	10.13	9.79	0.39	0.35	**0.91**	0.21	0.07	**0.78**	−0.23	**−0.54**	−0.26	0.57	0.56	−0.47	−0.36	**0.62**	0.12	0.42	**0.70**	0.14	0.02	**1.00**								
V	1.50	2.19	−0.35	0.34	−0.27	−0.13	−0.15	−0.40	**0.50**	−0.06	0.41	−0.15	−0.30	0.18	−0.17	−0.28	−0.35	−0.35	−0.07	−0.23	−0.18	−0.23	**1.00**							
Sr	9040.95	15748.61	0.21	**−0.69**	−0.05	0.08	0.23	0.09	−0.08	0.31	0.02	0.01	0.10	−0.13	0.00	−0.20	−0.25	−0.13	0.10	−0.14	**0.60**	−0.15	−0.21	**1.00**						
B	58.84	50.29	0.20	0.39	0.20	**0.74**	**0.55**	**0.75**	−0.29	−0.14	−0.28	**0.62**	**0.83**	−0.15	−0.32	**0.73**	0.08	**0.76**	−0.28	**0.90**	0.09	0.31	−0.23	−0.10	**1.00**					
As	0.82	0.32	0.18	0.03	0.14	−0.18	0.01	−0.06	0.02	0.43	0.14	−0.15	0.14	0.29	0.04	−0.23	0.37	0.48	0.00	−0.10	0.21	0.05	0.37	−0.21	0.14	**1.00**				
Ba	128.65	83.41	0.19	−0.41	−0.19	−0.36	0.07	**−0.53**	0.14	0.09	0.55	−0.22	−0.34	0.00	0.44	−0.48	0.09	**−0.56**	−0.08	−0.46	−0.34	−0.48	0.24	0.10	−0.49	0.16	**1.00**			
Al	10.44	22.84	−0.14	0.46	0.04	**0.80**	0.43	**0.69**	−0.30	−0.25	−0.14	**0.62**	**0.63**	−0.38	−0.17	**0.86**	0.12	0.44	−0.43	**0.98**	−0.22	0.19	−0.21	−0.14	**0.86**	−0.19	−0.43	**1.00**		
Zn	11.28	15.60	−0.32	0.02	−0.14	−0.26	−0.06	−0.33	−0.18	0.16	0.04	−0.15	−0.49	−0.09	−0.25	−0.22	−0.07	−0.36	−0.15	−0.30	−0.08	−0.12	−0.12	−0.10	−0.35	−0.30	−0.20	−0.26	**1.00**	
Fe	1123.96	2638.59	0.17	0.49	**0.74**	0.47	0.21	**0.86**	−0.33	**−0.65**	−0.13	**0.75**	**0.60**	−0.70	−0.25	**0.91**	0.18	0.30	0.37	0.49	−0.30	**0.86**	−0.28	−0.21	0.48	−0.21	−0.42	**0.58**	−0.16	**1.00**

Table 5. Pearson's correlation factor among physical–chemical parameters for major and trace elements of Mg-water samples. The significant direct and inverse correlations are shown in bold.

	Means	Std. Dev	Ca	Mg	K	Na	Cl	SO_4	HCO_3	SiO_2	pH	T	EC	Eh	Cr	Mn	Ni	Cu	U	Pb	Mo	Li	V	Sr	B	As	Ba	Al	Zn	Fe
Ca	56.25	13.76	**1.00**																											
Mg	46.96	8.21	0.41	**1.00**																										
K	1.65	0.78	−0.33	0.20	**1.00**																									
Na	47.97	24.16	0.12	0.41	−0.12	**1.00**																								
Cl	54.37	21.72	0.13	0.45	−0.14	**0.99**	**1.00**																							
SO_4	47.71	16.51	−0.04	0.29	−0.31	0.44	**0.54**	**1.00**																						
HCO_3	392.15	70.92	**0.62**	**0.78**	−0.08	0.65	**0.64**	0.10	**1.00**																					
SiO_2	28.78	8.26	−0.25	−0.42	−0.08	**−0.80**	**−0.75**	0.04	**−0.71**	**1.00**																				
pH	7.36	0.35	−0.41	0.01	−0.05	**0.67**	**0.67**	0.11	0.21	**−0.58**	**1.00**																			
T	20.07	2.63	0.14	**0.78**	0.30	0.31	0.29	0.05	**0.56**	−0.51	0.01	**1.00**																		
EC	876.55	167.90	0.34	**0.72**	−0.06	**0.84**	**0.87**	**0.52**	**0.84**	**−0.65**	0.37	0.50	**1.00**																	
EH	78.70	68.82	−0.13	−0.18	−0.29	0.24	0.23	−0.03	0.16	0.04	0.44	−0.46	0.16	**1.00**																
Cr	3.18	2.78	−0.32	−0.46	0.03	**−0.72**	**−0.70**	−0.38	**−0.51**	**0.68**	−0.21	−0.48	**−0.57**	0.36	**1.00**															
Mn	2.45	2.99	−0.09	−0.12	−0.35	0.51	0.46	0.38	0.10	−0.32	0.20	0.06	0.23	0.06	**−0.58**	**1.00**														
Ni	7.99	18.59	−0.10	−0.20	−0.47	−0.41	−0.32	0.07	−0.24	0.44	0.05	−0.45	−0.30	0.27	**0.55**	−0.30	**1.00**													
Cu	1.10	1.00	**0.52**	**0.71**	0.21	−0.08	−0.05	0.05	0.42	−0.19	−0.50	**0.74**	0.24	**−0.70**	−0.37	−0.13	−0.23	**1.00**												
U	1.47	0.74	−0.38	0.06	0.34	0.32	0.35	0.39	0.05	0.07	0.27	−0.21	0.38	**0.52**	0.10	0.06	−0.12	−0.44	**1.00**											
Pb	0.12	0.14	−0.37	−0.04	0.11	−0.17	−0.12	0.35	−0.40	0.18	−0.19	0.34	−0.12	**−0.55**	0.01	0.15	−0.16	0.31	−0.13	**1.00**										
Mo	1.42	2.07	0.14	−0.09	**−0.55**	0.41	0.47	**0.81**	−0.03	−0.03	0.03	−0.19	0.31	−0.07	−0.43	**0.59**	−0.03	−0.07	0.09	0.35	**1.00**									
Li	9.40	7.07	−0.24	**0.58**	0.26	**0.67**	**0.66**	0.16	**0.54**	**−0.64**	0.71	**0.63**	**0.67**	0.16	−0.30	0.01	−0.27	0.06	0.29	0.06	−0.17	**1.00**								
V	6.30	5.56	0.00	0.28	0.36	−0.45	−0.45	−0.25	−0.09	0.20	−0.38	**0.53**	−0.15	**−0.54**	0.28	**−0.63**	−0.10	**0.55**	−0.35	0.48	−0.43	0.16	**1.00**							
Sr	253.98	106.90	−0.50	0.10	0.30	0.15	0.17	**0.53**	−0.15	0.17	0.00	0.23	0.27	−0.01	0.05	0.20	−0.31	−0.04	**0.63**	**0.63**	0.27	0.32	0.18	**1.00**						
B	50.94	18.32	−0.37	0.45	0.28	**0.72**	**0.71**	0.46	0.40	−0.42	**0.58**	0.39	**0.70**	0.29	−0.36	0.31	−0.34	−0.14	**0.71**	0.02	0.09	**0.79**	−0.19	0.62	**1.00**					
As	0.82	0.34	**−0.59**	−0.02	0.38	−0.34	−0.32	0.13	−0.45	**0.63**	−0.12	−0.02	−0.22	0.16	0.50	−0.33	0.01	−0.20	0.49	0.32	−0.23	0.13	0.38	0.64	0.30	**1.00**				
Ba	20.53	19.72	−0.26	−0.23	−0.36	−0.41	−0.33	0.23	−0.32	**0.59**	−0.03	−0.44	−0.21	0.30	**0.66**	−0.31	**0.88**	−0.30	0.18	0.01	0.03	−0.21	0.00	0.10	−0.12	0.30	**1.00**			
Al	3.56	2.24	−0.05	−0.09	0.09	0.07	0.03	−0.12	−0.04	−0.29	−0.10	0.31	−0.13	−0.31	−0.35	**0.63**	−0.45	0.28	−0.31	0.45	0.16	−0.07	−0.10	0.09	−0.09	−0.28	−0.57	**1.00**		
Zn	14.20	25.88	0.23	−0.09	**−0.52**	0.08	0.13	**0.69**	−0.16	0.20	−0.35	−0.07	0.10	−0.36	−0.32	0.46	−0.05	0.18	−0.15	0.52	**0.90**	−0.38	−0.11	0.28	−0.16	−0.15	0.05	0.22	**1.00**	
Fe	10.67	7.39	−0.19	0.01	−0.12	0.46	0.35	−0.12	0.28	**−0.56**	0.39	0.36	0.21	0.09	−0.44	0.73	−0.31	−0.09	−0.09	−0.05	−0.03	0.35	−0.31	0.03	0.39	−0.33	−0.36	0.52	−0.12	**1.00**

As shown in Figure 4, Ca-HCO_3 waters highlighted a relatively high concentration of trace elements (Sr, Mn, Fe and Ba), whereas Mg-HCO_3 waters were characterized by relatively higher concentrations of elements such as Cr and Ni. The high concentrations of Fe and Mn, as previously stated, suggested a reducing condition established in a third system, outside the study area, directly connected with the phylladic basement, and where the mobilization of reduced species such as Fe^{2+} and Mn^{2+} is favored. High Sr concentrations were traced back to the dissolution of carbonates phases. For the Mg-HCO_3 group, slight enrichments in Cr and Ni were probably linked to the slight interaction with ultramafic rocks.

Moreover, to define the source of elements in waters and assess the expected relationships between elements by virtue of interactions with specific phases, correlations between major and trace elements for each group (Ca and Mg) were evaluated for the entire dataset (Tables 4 and 5) with a p-value of 0.05, including pH, temperature, EC, and Eh as additional parameters. The result of the correlation analysis showed a different constituent association for each group. In Ca-HCO_3 waters, EC was strongly associated with Ca, Na, Cl, HCO_3, and SO_4, indicating high conductivity of groundwater due to the presence of these ions. The presence of evaporitic levels (e.g., gypsum) in the Messinian successions, in addition to $CaCO_3$ as primary or secondary phase, can easily explain the high conductivities. In the Mg-HCO_3 group, Mg replaced Ca, highlighting a direct role of Mg-bearing phases during water–rock interaction. Furthermore, the Mg group exhibited a good correlation between Cr and Ni (not observed in Ca waters), in agreement with previous studies carried out in areas with ultramaphic rocks in [11,69–74] and a negative correlation between Cr, Ca, and Al, consistent with a direct interaction with ultramaphic rocks characterized by low concentrations of CaO and Al_2O_3 [75].

As reported by [11,69,70], for water interacting with ultramafic rocks, it is reasonable to expect a strong correlation between Mg, Cr, Ni, and Fe. Mg-HCO_3 waters of the Coreca area showed, as previously highlighted, a strong positive correlation between Cr and Ni and a slight negative correlation between these and Fe and Mg. Poor correlation can be related to secondary processes (precipitation), which tend to vary the relative ratios between each element [76].

Mg vs. Ni, Cr, and Mn diagrams (Figure 5) display the relationships between constituent directly linked to an interaction with ultramafic rocks. The diagrams show for all samples a general scatter of Ni and Cr more enriched in the Mg groups. In particular, the diagrams highlight a good correlation along the left side of each diagram-low salinity and low Mg concentration. The positive correlation is lost on the right side-high salinity and high Mg concentration-where the samples are oversaturated in calcite and with the highest salinities. For these groups, calcite precipitation could play an important role in the final composition. In fact, as reported by [76], trace elements are incorporated into the growing carbonate crystal. The authors highlighted that calcite can effectively sequester a variety of toxic cations from solution (e.g., Cd, Pb, Zn, Cu, Mn, Co, Fe, etc.) and trap them into the solid phase [76–78].

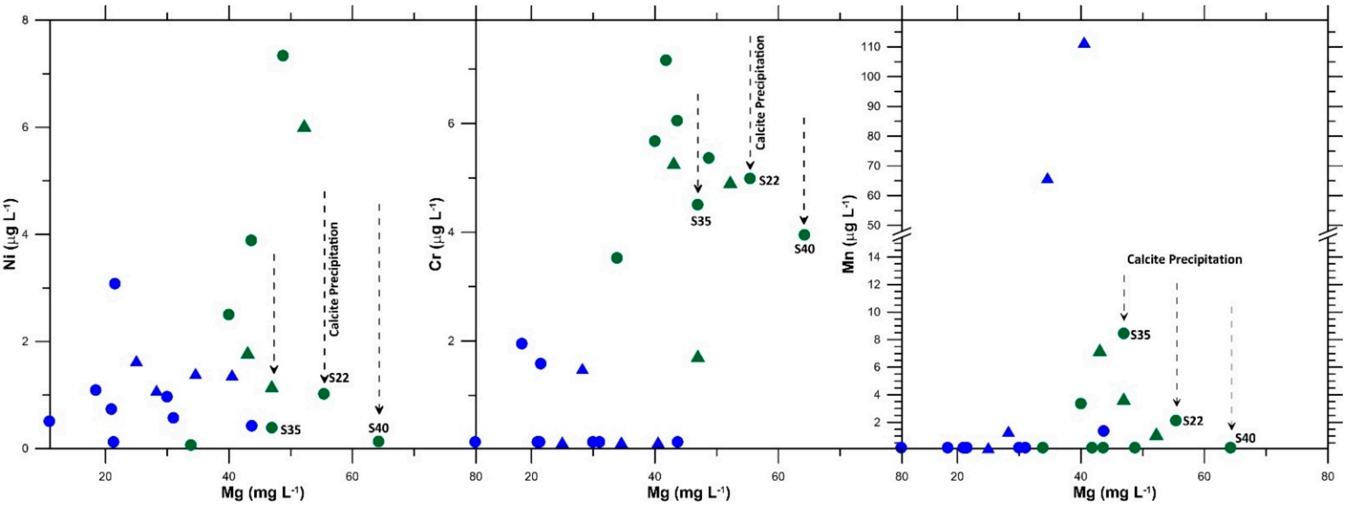

Figure 5. Correlation diagram of Ni vs. Mg, Cr vs. Mg, and Mn vs. Mg for the water samples from the Coreca area.

5. Groundwater Flow Interpretation

The absence of deep geological and hydrogeological surveys resulted in a speculative reconstruction of the groundwater system of the area. The hypothetic groundwater table was outlined using geological sections (Figures 6 and 7). Well and spring data revealed a multi-aquifer system, suggested by the presence of springs and a deep well (productive at about 30 m) close to each other. The occurrence of a multi-aquifer system was also supported by water chemistry indicating the coexistence of Ca-HCO_3 waters coming from a shallow Miocene–Quaternary aquifer, and Mg-HCO_3 waters from a deeper metamorphic aquifer (metabasalts and serpentinites).

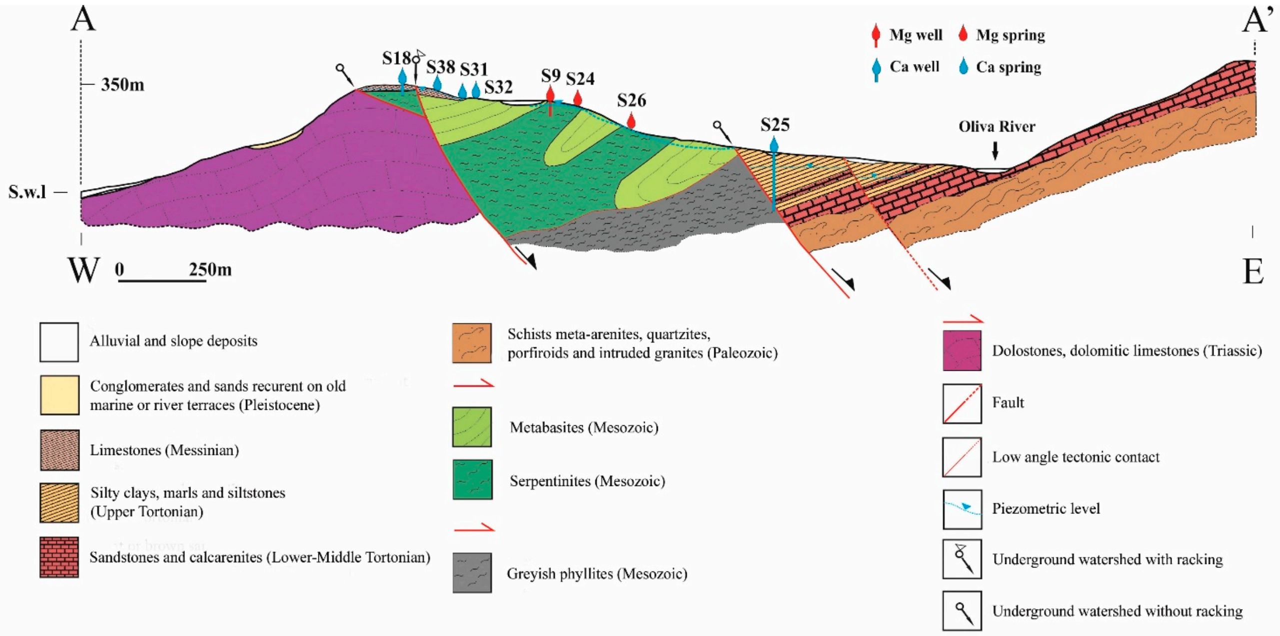

Figure 6. Geological–hydrogeological schematic cross-section A-A′ through the southern sector of the Coreca Area (modified after [79]). The trace of the section is shown in Figure 1.

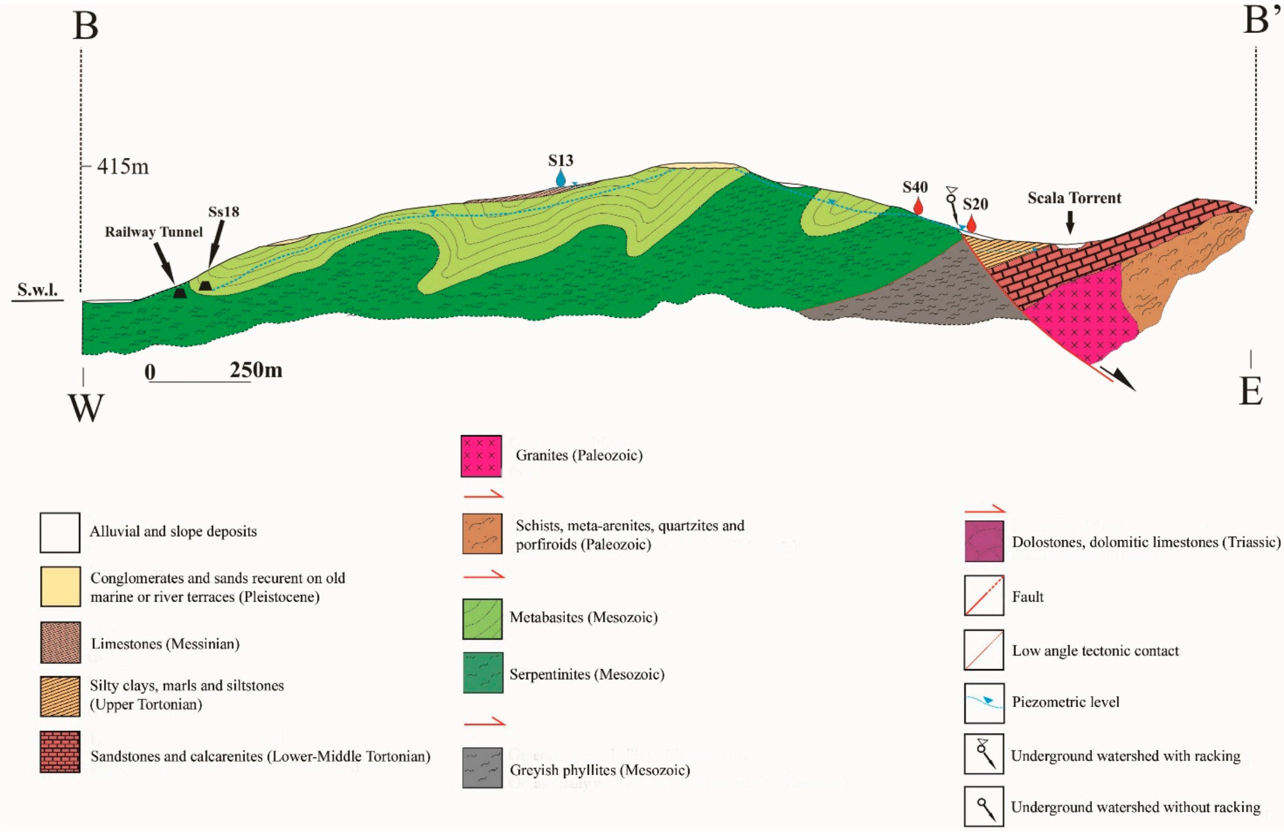

Figure 7. Geological–hydrogeological schematic cross-section (B-B') through the northern sector of Coreca Area. The trace of the section is shown in Figure 1.

Schematic cross sections A-A' and B-B' (Figures 6 and 7) show the presence of Ca^{2+}-enriched wells and springs both along the highest portions and the west side of the study area where the sedimentary Miocene succession outcrops. In the southern side, a permeability limit exists between the dolomitic (fractured and without springs) and the metamorphic rocks (with a high number of springs). Moreover, the schematic cross section B-B' (Figure 7) illustrates the multi-aquifer system and the differences between the west and east side of the studied area. A suspended Miocene carbonate aquifer occurs in the west side related to a permeability threshold with the metamorphic basement, whose flowrate is greater to the top of the area. On the east side, the metamorphic aquifer prevails, with the presence of Mg-HCO_3 waters. Metamorphic aquifer is well developed in the altered and fractured shallow portions that favor the water circulation. The east side is characterized by a permeability barrier, probably occurring between the metamorphic complex (metabasalts and serpentinites) and the underlying phyllites, and/or at the contact with the Miocene carbonate deposits. As reported in Section 4.3, the east downstream side (southern portion of the studied area) is pouring in Mg-HCO_3 waters. In this portion, the Mg aquifer is confined to the east by a normal fault system (N-S) representing a physical barrier to fluid flow (sealing fault zone) between the Tortonian–Messinian filling and the metamorphic basement (underground watershed without racking). Furthermore, the Upper Tortonian silty clays and siltstones, interbedded with the Tortonian sandstones and calcarenites, could play a buffering role not favoring the mixing between the two aquifers characterized by different chemical compositions.

6. Water Quality

Irrigation-water-quality parameters of the analyzed groundwater are shown in Table 6. Lastly, the general metal index (MI) was calculated to assess the water quality compared to metals in solution.

Table 6. Summary of irrigation-water parameters and their comparison with standard limits.

		SAR	SSP	MAR	KR	PS	EC
Mg-HCO$_3$	Mean	1.14	23.37	58.05	0.31	2.03	876.55
	Min	0.53	13.32	50.47	0.15	1.26	617
	Max	2.24	37.32	69.32	0.59	3.63	1178
Ca-HCO$_3$	Mean	0.95	20.75	31.15	0.25	2.1	937.25
	Min	0.54	13.67	14.23	0.15	1.02	660
	Max	1.61	29.71	43.05	0.41	4.13	1263
	Suitable	$10 < x < 18$	$40 < x < 60$	$x < 50$	$x \leq 1$	$x < 3$	
	Unsuitable	$x > 26$	$x > 80$	$x > 50$	$x \geq 1$	$x > 3$	

6.1. Salinity Hazard

The salinity hazard of irrigation water in terms of sodium adsorption ratio (SAR) is based on the relationship between Na ion and divalent cation [18]. It was determined using the following equation:

$$SAR = Na^+/[(Ca^{2+} + Mg^{2+}) \times 0.5]^{0.5} \tag{1}$$

Water with an SAR value < 10 is considered excellent; 10–18 is good; 18–26 is fair; and above 26 is unsuitable for irrigation use [24]. In the study area, all the samples were excellent for irrigation purpose, with maximum values < 2.5.

The suitability of groundwater for irrigation depends on the mineralization of water and its effect on plant and soil [80]. If the concentration of sodium is high in irrigation water, Na^+ tends to be absorbed by clay particles displacing Mg^{2+} and Ca^{2+} ions, thereby reducing soil permeability [80]. Sodium hazard based on SSP (soluble sodium percentage—SSP%) is useful in characterizing a water, since a high value indicates a soft water, and a low value indicates a hard water. It was calculated using the following equation:

$$SSP = [(Na^+ + K^+) \times 100]/(Ca^{2+} + Mg^{2+} + Na^+ + K^+) \tag{2}$$

If SSP is <20, the groundwater is excellent for irrigation; between 20 and 40 is good; between 40 and 60 is permissible; between 60 and 80 is doubtful and may be dangerous; and >80 is unsuitable for irrigation. The calculated values of SSP of the groundwater samples indicated that 100% of the water samples were excellent for irrigation purposes.

The SSP vs. EC plot [24] provides a method for rating irrigation water. In Figure 8a, the Coreca groundwater fell in the "excellent to good" and "good to permissible" fields. However, in the SAR vs. EC diagram (Figure 8b, [20]), the Coreca groundwater was ranked as C2-S1 and C3-S1 (medium to high salinity hazard and low sodium hazard). Excess salinity reduces the osmotic activity of plants, limiting the absorption of water and nutrients from the soil of exchangeable sodium [81].

Ca^{2+} and Mg^{2+} ions maintain a state of equilibrium in most groundwater [82]. In equilibrium, Mg^{2+} in water affects the soil by making it alkaline, affecting the final crop yield [83]. The measure of the effect of magnesium in irrigated water is expressed as the magnesium adsorption ratio (MAR). [84] developed an index for calculating the magnesium hazard. MAR is calculated using the formula:

$$MAR = (Mg^{2+} \times 100)/(Ca^{2+} + Mg^{2+}) \tag{3}$$

If the MAR value is <50, then the groundwater may be used for irrigation purposes; on the contrary, if it is >50, it is unsuitable. High magnesium content in groundwater induces an additional alkalizing effect. Usually, Ca^{2+} and Mg^{2+} are in equilibrium in most waters, [20,85] suggested that MAR values exceeding 50% indicate a magnesium hazard as the soil becomes more alkaline, resulting in decrease in the availability of phosphorous [86,87]. The results of the MAR calculation showed that 100% of the Ca-HCO$_3$

waters were suitable for irrigation purposes, whereas the Mg-HCO_3 waters highlighted values of between 50 and 60, indicating a magnesium hazard.

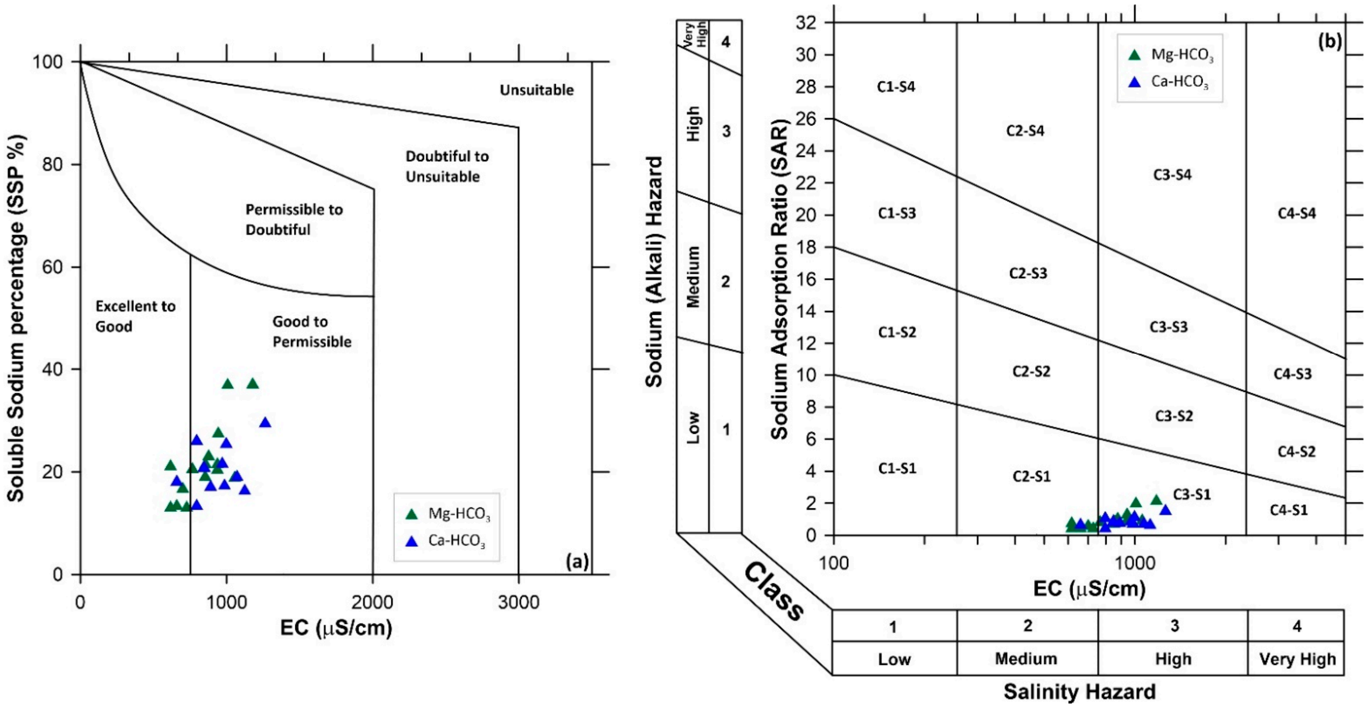

Figure 8. Plots of calculated values of (**a**) SSP and (**b**) SAR vs. EC of groundwater samples (diagrams for the classification of irrigation waters after [20,24]).

The Kelly ratio (KR) is an important parameter formulated by [19] based on the level of Na against Ca and Mg. It is expressed as:

$$KR = Na^{+} / (Ca^{2+} + Mg^{2+}) \quad (4)$$

Groundwater with a Kelly ratio <1.0 is considered suitable for irrigation purposes, while a KR value between 1 and 2 is classified as marginal and potentially dangerous for the groundwater, and if the KR is >2, then it is unsuitable. The KR value of the investigated groundwater showed that 100% of the samples were suitable for irrigation.

Lastly, the solubility of salts can be used to determine the potential salinity (PS). It is based on the sum of Cl^- and half of SO_4^{2-} concentrations [22], and is expressed as:

$$PS = Cl^{-} + \frac{1}{2} SO_4^{2-} \quad (5)$$

The Mg-HCO_3 and Ca-HCO_3 waters displayed PS values below 3, with only 3 cases (2 in Ca waters and 1 in Mg waters) with values between 3 and 4.

6.2. Metal Index (MI)

The metal index (MI) was used to assess the influence of overall pollution and illustrate the spatial distribution of heavy-metal concentration and the pollution index in the groundwater of the studied area [88].

The *MI* for drinking water was defined as:

$$MI = \sum_{i=1}^{N} \frac{C_i}{(MAC)_i}$$

where C is the concentration of each element in solution and i is the ith sample. For elements with concentration < detection limit (d.l.), C = d.l. was assumed. Therefore, MI was defined to evaluate the quality of the water based on the content of 13 metals. The higher the concentration of a metal compared to its respective maximum acceptable concentration (MAC) value, the worse the quality of the water. If the concentration of a specific element is higher than the respective MAC value ($MI > 1$), the water cannot be used according to law. The presence of several elements with concentrations smaller than but close to the respective MAC values will also decrease the overall quality of water because of an additive effect. Thus, an MI value > 1 is a threshold of warning.

Almost all samples showed MI values < 1, pointing to a good general quality of the resource (Table 2). Only S18, S25, S39, S20, S36, and S9 showed values of 1.03, 117.6, 155.2, 3.73, 1.06, and 1.2, respectively. S18, S36, and S9 had values close to 1 due to an overall high metal concentration relative to the entire dataset (additive effect). S20, S25, and S39 displayed a very high MI value, owing to the high concentration of a few specific constituents (Mn, Fe, and Ni). S25 and S39 were collected in deep wells where repeated alternations of reducing and oxidizing conditions can promote the release of Fe and Mn in solution. High Ni concentration detected in S20 (spring with $MgHCO_3$ composition) could be attributable both to prolonged interaction with ultramaphic rocks and/or localized anthropogenic pollution.

7. Conclusions

In the current study, hydrogeochemical characterization and statistical methods were used to investigate the groundwater quality and the origin of constituents (anthropic or natural) in groundwater of the Coreca area (Calabria, South Italy). Rock and water compositions were elaborated following statistical methods combined with hydrogeochemical modeling and conventional plots to investigate groundwater and related geochemical processes.

The mineral assemblage of the outcropping rocks and the multidisciplinary approach allowed the reconstruction of the water–rock interaction processes responsible for groundwater composition. Geochemical data and hydrogeological evidence confirmed the existence of two groups of groundwater: (a) Ca-HCO_3, hosted in the shallow Miocene/Quaternary aquifer, and (b) Mg-HCO_3 localized in the ultramaphic aquifer (serpentinites and metabasites). Calcite on the one hand and antigorite, tremolite, and clinochlore on the other represented the main phases that favored the formation of Ca and Mg systems.

The water–rock interaction with specific phases was confirmed by calculation of saturation indexes (SI), performed using PHREEQC Interactive software, and statistic elaboration. SI confirmed oversaturation with calcite, clinochlore, tremolite, and albite, and saturation with other phases characterizing the main outcropping lithotypes. Statistical approach allowed us to define, in Ca-HCO_3 waters, high concentrations of Sr, Mn, Fe, and Ba, with a strong correlation between EC and Ca, Na, Cl, HCO_3, and SO_4, indicating high conductivity of groundwater and direct interaction with carbonatic phases. In the Mg-HCO_3 group high concentrations in trace elements such as Cr and Ni were highlighted, and Mg replaced Ca, underlining a direct role of Mg-bearing phases during water–rock interaction. Furthermore, the Mg group exhibited a good correlation between Cr and Ni (not observed in Ca waters) and a negative correlation between Cr, Ca, and Al, in agreement with a direct interaction with ultramaphic rocks (e.g., serpentinite) characterized by low concentration in CaO and Al_2O_3.

Data confirmed a multi-aquifer system, as shown in the schematic cross sections that illustrate the differences between the west and east side of the studied area. A suspended Miocene/Quaternary carbonate aquifer occurs in the west side, related to a permeability threshold with the metamorphic basement, whose flowrate is greater to the top of the area. The east side is characterized by a permeability threshold, probably occurring between the metamorphic complex (metabasalts and serpentinites) and the underlying phyllites, and/or at the contact with the Miocene carbonate deposits. On the east side, the metamorphic aquifer prevails with the presence of Mg-HCO_3 waters, and it is well developed in the altered and fractured shallow portions that favor the circulation of water.

Subsequently, major and trace elements were compared with the Italian law limit values and the drinking water guidelines provided by World Health Organization (WHO, 2004). Only the S20, S25, and S39 samples showed Mn and Ni contents higher than the lowest threshold provided by Italian law (50 ppb and 20 ppb, respectively).

The salinity index SSP allowed us to classify the Coreca groundwater as "excellent to good" and "good to permissible"; nevertheless, a salinity problem and a magnesium hazard (east side) were found. This suggests that efforts, including leaching and proper drainage, are needed to control the salinity hazard, especially for those waters, representing a non-negligible part of the Coreca groundwater dataset, having an EC higher than 750 μS/cm. Moreover, the presence of a magnesium hazard suggests a need for long-term magnesium monitoring in the area to plan local alkalinity mitigation policies.

Lastly, calculation of the metal index (MI) revealed values <1 for almost all samples, testifying to a good general quality of the resource. Only a few samples had values much higher than 1, attributable to prolonged interaction with ultramaphic rocks and/or localized anthropogenic pollution.

From a general point of view, the data highlighted a good quality of groundwaters in the studied area (limited to the set of constituents analyzed), except for a few localized points and for limited exceedances of the maximum salinity thresholds, which must be monitored over time. Through a multidisciplinary approach, it was possible to ascertain the main anomalies attributable to the interaction with the hosting rocks and not (with few exceptions) to anthropic processes.

Author Contributions: Conceptualization, G.V., F.M. and C.A.; Data curation, G.V. and C.A.; Formal analysis, G.V. and C.A.; Investigation, G.V., F.M. and C.A.; Methodology, G.V., F.M. and C.A.; Project administration, F.M. and C.A.; Supervision, G.V., F.M. and C.A.; Validation, G.V., F.M. and C.A.; Visualization, G.V. and C.A.; Writing—original draft, G.V. and C.A.; Writing—review & editing, G.V., F.M. and C.A. All authors have read and agreed to the published version of the manuscript.

Funding: This research received no external funding. The APC was funded by all the authors.

Institutional Review Board Statement: Not applicable.

Informed Consent Statement: Not applicable.

Data Availability Statement: The manuscript is a data self-contained article, whose results were obtained from the laboratory analysis, and the entire data is presented within the article. However, if any additional information is required, these are available from the corresponding author upon request to the e-mail giovanni.vespasiano@unical.it.

Acknowledgments: The authors are extremely grateful to E. Vespasiano, M. Pulicicchio, and M. Cipriani for field assistance and for their special support during all work phases.

Conflicts of Interest: The authors declare no conflict of interest.

References

1. Appelo, C.A.J.; Postma, D. *Geochemistry, Groundwaters and Pollution*; A. A. Balkema: Rotterdam, The Netherlands, 1996; p. 536.
2. Stumm, W.; Morgan, J.J. *Aquatic Chemistry: Chemical Equilibrium and Rates in Natural Waters*, 3rd ed.; Wiley: New York, NY, USA, 1996; p. 1022.
3. Bocanegra, E.M.; Polemio, M.; Massone, H.E.; Dragone, V.; Limoni, P.P.; Farenga, M. A New Focus on Groundwater-Seawater Interactions. In *Indicators and Quality Classification Applied to Groundwater Management in Coastal Aquifers: Mar del Plata (Argentina) and Apulia (Italy) Case Studies*; Sanford, W., Langevin, C., Polemio, M., Povinec, P., Eds.; IAHS: Wallingford, UK, 2007; pp. 201–211.
4. Vardè, M.; Servidio, A.; Vespasiano, G.; Pasti, L.; Cavazzini, A.; Di Traglia, M.; Rosselli, A.; Cofone, F.; Apollaro, C.; Cairns, W.R.L.; et al. Ultra-trace determination of total mercury in Italian bottled waters. *Chemosphere* **2019**, *219*, 896–913. [CrossRef]
5. Vespasiano, G.; Apollaro, C. Preliminary geochemical characterization of a carbonate aquifer: The case of Pollino massif (Calabria, South Italy). *Rend. Online Soc. Geol. Ital.* **2016**, *38*, 109–112. [CrossRef]
6. Vespasiano, G.; Cianflone, G.; Cannata, C.B.; Apollaro, C.; Dominici, R.; De Rosa, R. Analysis of groundwater pollution in the Sant'Eufemia Plain (Calabria—South Italy). *Ital. J. Eng. Geol. Environ.* **2016**. [CrossRef]

7. Vespasiano, G.; Notaro, P.; Cianflone, G. Water-mortar interaction in a tunnel located in the Southern Calabria (Southern Italy). *Environ. Eng. Geosci.* **2018**, *24*, 305–315. [CrossRef]
8. Vespasiano, G.; Cianflone, G.; Romanazzi, A.; Apollaro, C.; Dominici, R.; Polemio, M.; De Rosa, R. A multidisciplinary approach for sustainable management of a complex coastal plain: The case of Sibari Plain (Southern Italy). *Mar. Pet. Geol.* **2019**. [CrossRef]
9. Muhammad, S.; Shah, M.T.; Khan, S. Health risk assessment of heavy metals and their source apportionment in drinking water of Kohistan region, northern Pakistan. *Microchem. J.* **2011**, *98*, 334–343. [CrossRef]
10. Alaya, M.B.; Saidi, S.; Zemni, T.; Zargouni, F. Suitability assessment of deep groundwater for drinking and irrigation use in the Djeffara aquifers (Northern Gabes, south-eastern Tunisia). *Environ. Earth Sci.* **2014**, *71*, 3387–3421. [CrossRef]
11. Bompoti, N.; Chrysochoou, M.; Dermatas, D. Geochemical characterization of Greek ophiolitic environments using statistical analysis. *Environ. Process* **2015**. [CrossRef]
12. Critelli, T.; Vespasiano, G.; Apollaro, C.; Muto, F.; Marini, L.; De Rosa, R. Hydrogeochemical study of an ophiolitic aquifer: A case study of Lago (Southern Italy, Calabria). *Environ. Earth Sci.* **2015**, *74*, 533–543. [CrossRef]
13. Mallick, J.; Singh, C.K.; AlMesfer, M.K.; Kumar, A.; Khan, R.A.; Islam, S.; Rahman, A. Hydro-geochemical assessment of groundwater quality in Aseer Region, Saudi Arabia. *Water* **2018**, *10*, 1847. [CrossRef]
14. Apollaro, C. Geochemical Modeling of Water-Rock Interaction in the Granulite Rocks of Lower Crust in the Serre Massif (Southern Calabria, Italy). *Geofluids* **2019**. [CrossRef]
15. Fehdi, C.; Rouabhia, A.; Baali, F.; Boudoukha, A. The hydrogeochemical characterization of Morsott-El Aouinet aquifer, North-eastern Algeria. *Environ. Geol.* **2009**, *58*, 1611–1620. [CrossRef]
16. D.Lgs.152. Decreto Legislativo 3 Aprile 2006, n. 152, Norme in Materia Ambientale. Gazzetta Ufficiale n. 88 del 14 Aprile 2006. Supplemento Ordinario n. 96. 2006. Available online: https://www.camera.it/parlam/leggi/deleghe/06152dl.htm (accessed on 15 January 2021).
17. WHO. *Guidelines for Drinking-Water Quality*, 4th ed.; World Health Organization: Geneva, Switzerland, 2011.
18. Richards, L.A. Diagnosis and improvement of saline alkali soils. In *Agriculture, 160. Handbook 60*; Department of Agriculture: Washington, DC, USA, 1954.
19. Kelley, W.P. Permissible composition and concentration of irrigation water. *Proc. Am. Soc. Civ. Eng.* **1940**, *66*, 607–613.
20. Raghunath, H.M. *Groundwater*; Wiley: New Delhi, India, 1987; p. 563.
21. Todd, D.K.; Mays, L.W. *Groundwater Hydrology*, 3rd ed.; Wiley: New York, NY, USA, 2005.
22. Doneen, L.D. *Notes on Water Quality in Agriculture*; Department of Water Science and Engineering, University of California: Davis, CA, USA, 1964.
23. Adewumi, A.J.; Anifowose, A.Y.B.; Olabode, F.O.; Laniyan, T.A. Hydrogeochemical Characterization and Vulnerability Assessment of Shallow Groundwater in Basement Complex Area, Southwest Nigeria. Contemp. *Trends Geosci.* **2018**, *7*, 72–103. [CrossRef]
24. Wilcox, L.V. *Classification and Use of Irrigation Waters*; USDA. Circ 969: Washington, DC, USA, 1955.
25. Salifu, M.; Aidoo, F.; Saah Hayford, M.; Adomako, D.; Asare, E. Evaluating the suitability of groundwater for irrigational purposes in some selected districts of the Upper West region of Ghana. *Appl. Water Sci.* **2017**. [CrossRef]
26. Rawat, K.S.; Singh, S.K.; Gautam, S.K. Assessment of groundwater quality for irrigation use: A peninsular case study. *Appl. Water Sci.* **2018**, *8*, 233. [CrossRef]
27. Van Dijk, J.P.; Bello, M.; Brancaleoni, G.P.; Cantarella, G.; Costa, V.; Frixia, A.; Golfetto, F.; Merlini, S.; Riva, M.; Torricelli, S.; et al. A regional structural model for the northern sector of the Calabrian Arc (southern Italy). *Tectonophysics* **2000**, *324*, 267–320. [CrossRef]
28. Critelli, S.; Muto, F.; Tripodi, V.; Perri, F.; Schattner, U. Relationships between lithospheric flexure, thrust tectonics and stratigraphic sequences in foreland setting: The Southern Apennines foreland basin system, Italy. *Tectonics* **2011**, *2*, 121–170.
29. Critelli, S.; Muto, F.; Perri, F.; Tripodi, V. Interpreting provenance relations from sandstone detrital modes, southern Italy foreland region: Stratigraphic record of the Miocene tectonic evolution. *Mar. Petrol. Geol.* **2017**, *87*, 1–13. [CrossRef]
30. Cirrincione, R.; Fazio, E.; Fiannacca, P.; Ortolano, G.; Pezzino, A.; Punturo, R. The Calabria-Peloritani Orogen, a composite terrane in Central Mediterranean; its overall architecture and geodynamic significance for a pre-Alpine scenario around the Tethyan basin. Progresses in Deciphering Structures and Compositions of Basement Rocks. *Period. Mineral.* **2015**, *84*, 701–749. [CrossRef]
31. Bonardi, G.; Cello, G.; Perrone, V.; Tortorici, L.; Turco, E.; Zuppetta, A. The evolution of the northern sector of the Calabria–Peloritani Arc in a semiquantitative palynspastic restoration. *Boll. Soc. Geol. Ital.* **1982**, *101*, 259–274.
32. Bonardi, G.; Giunta, G.; Perrone, V.; Russo, M.; Zuppetta, A.; Ciampo, G. Osservazioni sull'evoluzione dell'Arco Calabro-Peloritano nel Miocene inferiore: La Formazione di Stilo-Capo d'Orlando. *Boll. Soc. Geol. Ital.* **1980**, *99*, 365–393.
33. Tortorici, L. Lineamenti geologico-strutturali dell'arco calabro-peloritano. *Rend. SIMP* **1982**, *38*, 927–940.
34. Boccaletti, M.; Nicolich, R.; Tortorici, L. The Calabrian Arc and the Ionian Sea in the dynamic evolution of the Central Mediterranean. *Mar. Geol.* **1984**, *55*, 219–245. [CrossRef]
35. Tansi, C.; Muto, F.; Critelli, S.; Iovine, G. Neogene-Quaternary strike-slip tectonics in the central Calabrian Arc (southern Italy). *J. Geodyn.* **2004**, *43*, 393–414. [CrossRef]
36. Tansi, C.; Folino Gallo, M.; Muto, F.; Perrotta, P.; Russo, L.; Critelli, S. Seismotectonics and landslides of the Crati Graben (Calabrian Arc, Southern Italy). *J. Maps* **2016**, *12*, 363–372. [CrossRef]

37. Brutto, F.; Muto, F.; Loreto, M.F.; De Paola, N.; Tripodi, V.; Critelli, S.; Facchin, L. The Neogene-Quaternary geodynamic evolution of the central Calabrian Arc: A case study from the western Catanzaro Trough basin. *J. Geodyn.* **2016**, *102*, 95–114. [CrossRef]
38. Tripodi, V.; Muto, F.; Brutto, F.; Perri, F.; Critelli, S. Neogene-Quaternary evolution of the forearc and backarc regions between the Serre and Aspromonte Massifs, Calabria (southern Italy). *Mar. Pet. Geol.* **2018**, *95*, 328–343. [CrossRef]
39. Ogniben, L. Schema introduttivo alla geologia del confine calabro-lucano. *Mem. Soc. Geol. Ital.* **1969**, *8*, 453–763.
40. Iannace, A.; Bonardi, G.; D'Errico, M.; Mazzoli, S.; Perrone, V.; Vitale, S. Structural setting and tectonic evolution of the Apennine Units of northern Calabria. *Comptes Rendues Geosci.* **2005**, *337*, 1541–1550. [CrossRef]
41. Iannace, A.; Garcia Tortosa, F.J.; Vitale, S. The Triassic metasedimentary successions across the boundary between Southern Apennines and Calabria–Peloritani Arc (Northern Calabria, Italy). *Geol. J.* **2005**, *40*, 155–171. [CrossRef]
42. Iannace, A.; Vitale, S.; D'Errico, M.; Mazzoli, S.; Di Staso, A.; Macaione, E.; Messina, A.; Reddy, S.M.; Somma, R.; Zamparelli, V.; et al. The carbonate tectonic units of northern Calabria (Italy): A record of Apulian palaeomargin evolution and Miocene convergence, continental crust subduction, and exhumation of HP–LT rocks. *J. Geol. Soc.* **2007**, *164*, 1165–1186. [CrossRef]
43. Scandone, P. Structure and evolution of the Calabrian Arc. *Earth Evol. Sci.* **1982**, *3*, 172–180.
44. Muto, F.; Perri, E. Evoluzione tettono-sedimentaria del bacino di Amantea, Calabria occidentale. *Boll. Soc. Geol. Ital.* **2002**, *121*, 391–409.
45. Longhitano, S.G.; Nemec, W. Statistical analysis of bed-thickness variation in a Tortonian succession of biocalcarenitic tidal dunes, Amantea Basin, Calabria, southern Italy. *Sediment. Geol.* **2005**, *179*, 195–224. [CrossRef]
46. Muto, F.; Critelli, S.; Robustelli, G.; Tripodi, V.; Zecchin, M.; Fabbricatore, D.; Perri, F. A Neogene-Quaternary Geotraverse within the northern Calabrian Arc from the foreland peri- Ionian margin to the back-arc Tyrrhenian margin. Periodico semestrale del Servizio Geologico d'Italia—ISPRA e della Società Geologica Italiana. *Geol. Field Trips* **2015**, *7*, 1–65. [CrossRef]
47. Borrelli, L.; Muto, F. Geology and mass movements of the Licetto River catchment (Calabrian Coastal Range, Southern Italy). *J. Maps* **2017**, *13*, 588–599. [CrossRef]
48. Costanzo, A.; Cipriani, M.; Feely, M.; Cianflone, G.; Dominici, R. Messinian twinned selenite from the Catanzaro Trough, Calabria, Southern Italy: Field, petrographic and fluid inclusion perspectives. *Carbonates Evaporites* **2019**, *34*, 743–756. [CrossRef]
49. Corbi, F.; Fubelli, G.; Lucà, F.; Muto, F.; Pelle, T.; Robustelli, G.; Scarciglia, F.; Dramis, F. Vertical movements in the Ionian margin of the Sila Massif (Calabria, Italy). *Boll. Soc. Geol. Ital.* **2009**, *128*, 731–738.
50. Muto, F.; Spina, V.; Tripodi, V.; Critelli, S.; Roda, C. Neogene tectonostratigraphic evolution of allochthonous terranes in the eastern Calabrian foreland (southern Italy). *Ital. J. Geosci.* **2014**, *133*, 455–473. [CrossRef]
51. Zecchin, M.; Civile, D.; Caffau, M.; Critelli, S.; Muto, F.; Mangano, G.; Ceramicola, S. Sedimentary evolution of the Neogene-Quaternary Crotone Basin (southern Italy) and relationships with large-scale tectonics: A sequence stratigraphic approach. *Mar. Pet. Geol.* **2020**, *117*, 104381. [CrossRef]
52. Piluso, E.; Cirrincione, R.; Morten, L. Ophiolites of the calabrian peloritan arc and their relationships with the crystalline basement (Catena Costiera and Sila Piccola, Calabria, southern Italy). *Ofioliti Glom Excursion Guideb.* **2000**, *25*, 117–140.
53. Bloise, A.; Miriello, D.; De Rosa, R.; Vespasiano, G.; Fuoco, I.; De Luca, R.; Barrese, E.; Apollaro, C. Mineralogical and geochemical characterization of birnessite, ranciéite and asbestiform todorokite from Serra D'Aiello (Southern-Italy). *Fibers* **2020**, *8*, 9. [CrossRef]
54. Allocca, V.; Celico, F.; Celico, P.; De Vita, P.; Fabbrocino, S.; Mattia, S.; Monacelli, G.; Musilli, I.; Piscopo, V.; Scalise, A.R.; et al. *Note Illustrative Della Carta Idrogeologica dell'Italia Meridionale*; Istituto Poligrafico e Zecca dello Stato: Rome, Italy, 2007; ISBN1 88-448-0215-5. p. 211, con carte allegate; ISBN2 88-448-0223-6.
55. Apollaro, C.; Vespasiano, G.; Muto, F.; De Rosa, R.; Barca, D.; Marini, L. Use of mean residence time of water, flowrate, and equilibrium temperature indicated by water geothermometers to rank geothermal resources. Application to the thermal water circuits of Northern Calabria. *J. Volcanol. Geotherm. Res.* **2016**, *328*, 147–158. [CrossRef]
56. Apollaro, C.; Tripodi, V.; Vespasiano, G.; De Rosa, R.; Dotsika, E.; Fuoco, I.; Critelli, S.; Muto, F. Chemical, isotopic and geotectonic relations of the warm and cold waters of the Galatro and Antonimina thermal areas, southern Calabria, Italy. *Mar. Pet. Geol.* **2019**, *109*, 469–483. [CrossRef]
57. Apollaro, C.; Caracausi, A.; Paternoster, M.; Randazzo, P.; Aiuppa, A.; De Rosa, R.; Fuoco, I.; Mongelli, G.; Muto, F.; Vannia, E.; et al. Fluid geochemistry in a low-enthalpy geothermal field along a sector of southern Apennines chain (Italy). *J. Geochem. Explor.* **2020**. [CrossRef]
58. Vespasiano, G.; Apollaro, C.; Muto, F.; Dotsika, E.; De Rosa, R.; Marini, L. Chemical and isotopic characteristics of the warm and cold waters of the Luigiane Spa near Guardia Piemontese (Calabria, Italy) in a complex faulted geological framework. *Appl. Geochem.* **2014**, *41*, 73–88. [CrossRef]
59. Vespasiano, G.; Apollaro, C.; De Rosa, R.; Muto, F.; Larosa, S.; Fiebig, J.; Mulch, A.; Marini, L. The Small Spring Method (SSM) for the definition of stable isotope—elevation relationships in Northern Calabria (Southern Italy). *Appl. Geochem.* **2015**, *63*, 333–346. [CrossRef]
60. Vespasiano, G.; Marini, L.; Apollaro, C.; De Rosa, R. Preliminary geochemical characterization of the thermal waters of Caronte SPA springs (Calabria, South Italy). *Rend. Online Soc. Geol. Ital.* **2016**, *39*, 138–141.
61. Nordstrom, D.K. Thermochemical redox equilibria of ZoBell's solution. *Geochim. Cosmochim. Acta* **1997**, *41*, 1835–1841. [CrossRef]
62. Nollet, L.M.L.; De Gelder, L.S.P. *Handbook of Water Analysis*; CRC Press: Boca Raton, FL, USA, 2007; p. 944.

63. Parkhurst, D.L.; Appelo, C.A.J. Description of Input and Examples for PHREEQC Version 3- a Computer Program for Speciation, Batch-Reaction, One-Dimensional Transport, and Inverse Geochemical Calculations. U.S. Geological Survey Techniques and Methods, Book 6, Chap. A43; 2013; p. 497. Available online: http://pubs.https://pubs.usgs.gov/tm/06/a43// (accessed on 15 January 2021).
64. Apollaro, C.; Fuoco, I.; Brozzo, G.; De Rosa, R. Release and fate of Cr (VI) in the ophiolitic aquifers of Italy: The role of Fe (III) as a potential oxidant of Cr (III) supported by reaction path modelling. *Sci. Total Environ.* **2019**, *660*, 1459–1471. [CrossRef]
65. Apollaro, C.; Accornero, M.; Marini, L.; Barca, D.; De Rosa, R. The impact of dolomite and plagioclase weathering on the chemistry of shallow groundwaters circulating in a granodiorite-dominated catchment of the Sila Massif (Calabria, Southern Italy). *Appl. Geochem.* **2009**, *24*, 957–979. [CrossRef]
66. Apollaro, C.; Buccianti, A.; Vespasiano, G.; Vardè, M.; Fuoco, I.; Barca, D.; Bloise, A.; Miriello, D.; Cofone, F.; Servidio, A.; et al. Comparative geochemical study between the tap waters and the bottled mineral waters in Calabria (southern Italy) by compositional data analysis (CoDA) developments. *Appl. Geochem.* **2019**, *107*, 19–33. [CrossRef]
67. Lacinska, A.M.; Styles, M.T.; Bateman, K.; Wagner, D.; Hall, M.R.; Gowing, C.; Brown, P.D. Acid-dissolution of antigorite, chrysotile and lizardite for ex situ carbon capture and storage by mineralisation. *Chem. Geol.* **2016**, *437*, 153–169. [CrossRef]
68. Marini, L.; Ottonello, G. *Atlante degli acquiferi della Liguria. Volume III: Le acque dei complessi ofiolitici (bacini: Arrestra, Branega, Cassinelle, Cerusa, Erro, Gorzente, Leira, Lemme, Lerone, Orba, Piota, Polcevera, Rumaro, Sansobbia, Stura, Teiro, Varenna, Visone)*; Pacini: Pisa, Italy, 2002.
69. Oze, C.; Fendorf, S.; Bird, D.K.; Coleman, R.G. Chromium geochemistry of serpentine soils. *Int. Geol. Rev.* **2004**. [CrossRef]
70. Kelepertsis, A.; Alexakis, D.; Kita, I. Environmental geochemistry of soils and waters of Susaki area, Korinthos, Greece. *Environ. Geochem. Health* **2001**. [CrossRef]
71. Apollaro, C.; Marini, L.; De Rosa, R. Use of reaction path modeling to predict the chemistry of stream water and groundwater: A case study from the Fiume Grande valley (Calabria, Italy). *Environ. Geol.* **2007**, *51*, 1133–1145. [CrossRef]
72. Apollaro, C.; Marini, L.; De Rosa, R.; Settembrino, P.; Scarciglia, F.; Vecchio, G. Geochemical features of rocks, stream sediments, and soils of the Fiume Grande Valley (Calabria, Italy). *Environ. Geol.* **2007**, *52*, 719–729. [CrossRef]
73. Apollaro, C.; Marini, L.; Critelli, T.; Barca, D.; Bloise, A.; De Rosa, R.; Liberi, F.; Miriello, D. Investigation of rock-to-water release and fate of major, minor, and trace elements in the metabasalt-serpentinite shallow aquifer of Mt. Reventino (CZ, Italy) by reaction path modeling. *Appl. Geochem.* **2011**, *26*, 1722–1740. [CrossRef]
74. Apollaro, C.; Fuoco, I.; Vespasiano, G.; De Rosa, R.; Cofone, F.; Miriello, D.; Bloise, A. Geochemical and mineralogical characterization of tremolite asbestos contained in the Gimigliano-Monte Reventino Unit (Calabria, south Italy). *J. Mediterr. Earth Sci.* **2018**, *10*, 5–15.
75. Dichicco, M.C.; Laurita, S.; Paternoster, M.; Rizzo, G.; Sinisi, R.; Mongelli, G. Serpentinite Carbonation for CO2 Sequestration in the Southern Apennines: Preliminary Study. *Energy Procedia* **2015**, *76*, 477–486. [CrossRef]
76. Rimstidt, J.D.; Balog, A.; Webb, J. Distribution of trace elements between carbonate minerals and aqueous solutions. *Geochim. Cosmochim. Acta* **1998**, *62*, 1851–1863. [CrossRef]
77. Drake, H.; Mathurin, F.A.; Zack, T.; Schäfer, T. Incorporation of Trace Elements into Calcite Precipitated from Deep Anoxic Groundwater in Fractured Granitoid Rocks. *Procedia Earth Planet. Sci.* **2017**, *17*, 841–844. [CrossRef]
78. Ettler, V.; Zelená, O.; Mihaljevič, M.; Šebek, O.; Strnad, L.; Coufal, P.; Bezdička, P. Removal of trace elements from landfill leachate by calcite precipitation. *J. Geochem. Explor.* **2006**, *88*, 28–31. [CrossRef]
79. Vespasiano, G.; Apollaro, C.; Muto, F.; De Rosa, R. Geochemical and hydrogeological characterization of the metamorphic-serpentinitic multiaquifer of the Scala catchment, Amantea (Calabria, South Italy). *Rend. Online Soc. Geol. Ital.* **2012**, *21*, 879–880.
80. Selvakumar, S.; Chandrasekar, N.; Srinivas, Y.; Simon-peter, T.; Magesh, N.S. Evaluation of the groundwater quality along coastal stretch between Vembar and Taruvaikulam, Tamil Nadu, India: A statistical approach. *J. Coast. Sci.* **2014**, *1*, 22–26.
81. Subramani, T.; Elango, L.; Damodarasamy, S.R. Groundwater quality and its suitability for drinking and agricultural use in Chithar River Basin, Tamil Nadu, India. *Environ. Geol.* **2005**, *47*, 1099–1110. [CrossRef]
82. Hem, J.D. *Study and Interpretation of the Chemical Characteristics of Natural Water (Vol. 2254)*; Department of the Interior, US Geological Survey: Reston, VA, USA, 1985.
83. Kumar, P.K.; Gopinath, G.; Seralathan, P. Application of remote sensing and GIS for the demarcation of groundwater potential zones of a river basin in Kerala, southwest coast of India. *Int. J. Remote Sens.* **2007**, *28*, 5583–5601. [CrossRef]
84. Paliwal, K.V. Irrigation with saline water. In *Monogram no. 2 (New Series)*; IARI: New Delhi, India, 1972; p. 198.
85. Gupta, S.K.; Gupta, I.C. *Management of Saline Soils and Water*; Oxford and IBM Publ. Co: New Delhi, India, 1987.
86. Gautam, S.K.; Maharana, C.; Sharma, D.; Singh, A.K.; Tripathi, J.K.; Singh, S.K. Evaluation of groundwater quality in the Chotanagpur Plateau region of the Subarnarekha River Basin, Jharkhand State, India. *Sustain. Water Qual. Ecol.* **2015**, *6*, 57–74. [CrossRef]
87. Al-Shammiri, M.; Al-Saffar, A.; Bohamad, S.; Ahmed, M. Wastewater quality and reuse in irrigation in Kuwait using microfiltration technology in treatment. *Desalination* **2005**, *185*, 213–225. [CrossRef]
88. Tamasi, G.; Cini, R. Heavy metals in drinking waters from Mount Amiata (Tuscany, Italy). Possible risks from arsenic for public health in the Province of Siena. *Sci. Total Environ.* **2004**, *327*, 41–51. [CrossRef] [PubMed]